Optimal and Robust Beamforming for Secure Transmission in MISO Visible-Light Communication Links

Ayman Mostafa, *Student Member, IEEE,* and Lutz Lampe, *Senior Member, IEEE*

***Abstract*—This work considers secure downlink transmission in indoor multiple-input, single-output (MISO) visible-light communication (VLC) links. In particular, we study the design of transmit beamformers that maximize the achievable secrecy rate subject to amplitude constraints imposed by the limited dynamic range of the light-emitting diodes (LEDs). Such constraints render the design problem nonconvex and difficult to solve. We show, however, that this nonconvex problem can be transformed into a solvable quasiconvex line search problem. We also consider the more realistic case of imperfect channel information regarding the receiver's and eavesdropper's links. We tackle the worst-case secrecy rate maximization problem, again subject to amplitude constraints. In our treatment, uncertainty in the receiver's channel is due to limited feedback, and is modelled by spherical sets. On the other hand, there is no feedback from the eavesdropper, and the transmitter shall utilize the line-of-sight (LoS) channel gain equation to map the eavesdropper's nominal location and orientation into an estimate of the channel gain. Thus, we derive uncertainty sets based on inaccurate information regarding the eavesdropper's location and orientation, as well as the emission pattern of the LEDs. We also consider channel mismatches caused by the uncertain non-line-of-sight (NLoS) components. We provide numerical examples to demonstrate the performance gain of the optimal beamformer compared to suboptimal schemes, and the robust beamformer compared to its non-robust counterparts. We also evaluate the worst-case secrecy rate performance of the robust beamformer in a typical VLC scenario along with the aforementioned uncertainty sources.**

***Index Terms*—physical-layer security, visible-light communications, amplitude constraints, robust beamforming, worst-case secrecy rate.**

I. Introduction

INFORMATION-THEORETIC security was pioneered by Wyner back in the mid-1970s with his seminal work [1] that introduced the wiretap channel model and the notion of secrecy capacity as a performance metric for reliable and secure communications. Almost three decades after, interest in physical-layer security has been revived by the need for additional secrecy measures that do not jeopardize low complexity at the receiver. In physical-layer security systems, the transmitter exploits dissimilarities among the channels of different receivers and adopts signaling and/or coding schemes that ensure reliable reception by the intended receivers and, at the same time, hinder unintended or unauthorized receivers from inferring the transmitted messages [2]–[5]. Nevertheless, the secrecy performance of physical-layer security systems can severely deteriorate by inaccurate channel information, especially if the unintended receiver is a malicious user or passive eavesdropper attempting to hide its presence from the transmitter. Performance sensitivity, however, can be alleviated by adopting transmission schemes that explicitly take channel uncertainty into account. Such schemes are typically referred to as *robust transmission schemes*.

Visible-light communication (VLC) is a wireless transmission technology that exploits illumination devices, mostly high-brightness light-emitting diodes (LEDs), for short-range data connectivity [6]. In VLC systems, information is relayed by the means of modulating the output intensity of the LEDs, whereas at the receiver side, the data signal is recovered using simple photodetectors. Typical lighting systems utilize multiple LEDs to provide uniform illumination. Thus, VLC systems can readily benefit from multiple-antenna techniques to enhance the reliability and/or security of VLC networks. Being a broadcast channel, data transmitted over VLC links are inherently vulnerable to overhearing by unintended receivers or eavesdroppers existing in the service area illuminated by the transmit LEDs. Therefore, secure transmission in VLC systems using physical-layer security techniques has been proposed in [7].

In this paper, we consider the design of transmit beamformers for secure downlink transmission in indoor multiple-input, single-output (MISO) VLC links in the presence of a passive eavesdropper attempting to overhear information conveyed by light waves to the legitimate receiver. Assuming uniform input distribution, our performance measure is the secrecy rate expression derived in [7] for amplitude-constrained wiretap channels. Under the premise of perfect channel information, we first consider the design of *optimal* beamformers that maximize the achievable secrecy rate subject to amplitude constraints. Such constraints render the optimization problem nonconvex and difficult to solve. Nevertheless, we show that this nonconvex problem can be recast as a solvable quasiconvex line search problem. Next, we consider the more general and more realistic case in which the transmitter has uncertain information regarding the receiver's and eavesdropper's channels. We study the design of *robust* beamformers that maxi-

Manuscript received March 7, 2016; revised July 12, 2016; accepted August 12, 2016. This work was supported by the Natural Sciences and Engineering Research Council of Canada (NSERC). A preliminary version of a portion of this material was presented at the 2015 ICC Workshop in Visible Light Communications and Networking (VLCN), London, UK, June 2015.

A. Mostafa and L. Lampe are with the Department of Electrical and Computer Engineering, The University of British Colombia, Vancouver, BC, V6T 1Z4, Canada (emails: amostafa@ece.ubc.ca; lampe@ece.ubc.ca).

mize the worst-case secrecy rate, again subject to amplitude constraints. The resulting max-min problem is more complex than its non-robust counterpart but still can be transformed into a quasiconvex line search problem. The tractability of this problem, however, depends on the geometries of the uncertainty sets. For the receiver's channel, we consider uncertainty arising from quantization errors imposed by the finite rate of the feedback channel. Such uncertainty is well modelled with N-dimensional spherical sets centered at the nominal estimate available to the transmitter, where N is the number of transmit elements. For the eavesdropper's channel, however, we do not assume any feedback because the eavesdropper is a passive or non-cooperative receiver. Instead, we take advantage of the fact that the line-of-sight (LoS) path is typically dominant in VLC channels. Moreover, the LoS channel gain can be accurately approximated by a deterministic function of the receiver's location and orientation, along with the emission pattern of the LEDs. In typical VLC scenarios, it is sensible to assume that the transmitter has some knowledge of the receiver's location and orientation. Thus, a reasonable estimate of the eavesdropper's channel can be obtained from such information. Accordingly, we derive uncertainty sets that reflect the transmitter's imprecise knowledge of the eavesdropper's location and orientation, as well as the emission pattern of the LEDs. We also consider possible channel mismatches caused by non-line-of-sight (NLoS) components. Such components are due to diffuse reflections from nearby surfaces, and are not taken into account by the LoS channel gain equation. All the derived uncertainty sets are well structured in the sense that they result in solvable worst-case secrecy rate maximization problems.

The secrecy performance of the Gaussian MISO wiretap channel with perfect channel information, subject to a total average power constraint, was studied in [8]–[11]. Lower bounds on the secrecy capacity were obtained in [8] and [9]. In addition, it was shown in [9] that beamforming is the optimal transmission strategy if the channel inputs are Gaussian. These results were generalized in [10] and [11] where it was shown that Gaussian signaling, along with beamforming, is in fact optimal, and closed-form secrecy capacity expressions were derived. The design of robust transmission schemes with imperfect channel information, based on worst-case secrecy rate maximization, was considered in [12]–[17]. In [12], the authors observed similarities between the cognitive radio and wiretap channel models, and considered the design of robust beamformers in conjunction with spherical uncertainty sets for the eavesdropper's channel. The authors in [13] studied robust beamforming along with discrete uncertainty sets corresponding to inaccurate information regarding the eavesdropper's location, under the assumption of LoS propagation. Worst-case secrecy rate maximization for the MISO channel wiretapped by multiple, multi-antenna eavesdroppers was considered in [14] using spherical uncertainty sets for the receiver's and eavesdroppers' channels. In [15], the authors considered the use of artificial noise generated by a friendly jammer and studied the design of robust data and jamming covariance matrices, under both individual and global power constraints. The work in [16] considered the design of robust transmit covariance matrices for the multiple-input, multiple-output (MIMO) wiretap channel, in the low signal-to-noise ratio (SNR) regime, using a linearized secrecy rate expression, i.e., the secrecy rate is approximated by a linear function of the covariance matrix. A similar approach was utilized in [17] where the data and jamming covariance matrices are alternatively optimized after linearizing the nonconcave term in the secrecy rate expression based on Taylor's first-order approximation.

Compared to the previously mentioned works, our work in this paper has the following two key differences:

1) We design the beamformer $\mathbf{w}$ subject to a per-transmit-element amplitude constraint, i.e., $\|\mathbf{w}\|_\infty \leq 1$. Amplitude constraints explicitly arise in VLC systems because of the limited dynamic range of the LEDs, and they are usually difficult to handle. Furthermore, as a side advantage, our approach to solve the optimization problem is in fact applicable to general l_p-norm constraints, i.e., $\|\mathbf{w}\|_p \leq 1$, for any $p \geq 1$. On the other hand, the works in [8]–[17] consider a total power constraint P on the transmitted signal vector, i.e., $\|\mathbf{w}\|_2 \leq \sqrt{P}$, or more generally, $\mathbf{W} \succeq 0, \mathrm{Trace}(\mathbf{W}) \leq P$, where $\mathbf{W}$ is the transmit covariance matrix.
2) We do not assume channel feedback from the eavesdropper. Instead, we exploit the imprecise knowledge of the eavesdropper's location and orientation to obtain an estimate of the eavesdropper's channel gain. Specifically, we derive uncertainty sets for the eavesdropper's channel based on the uncertain parameters in the LoS channel gain equation. We also consider uncertainty caused by the NLoS components. On the other hand, the works in [12], [14]–[17] assume spherical uncertainty sets for the eavesdropper's channel, that is $\|\mathbf{h}_{\mathrm{E}} - \hat{\mathbf{h}}_{\mathrm{E}}\|_2 \leq \epsilon_{\mathbf{h}_{\mathrm{E}}}$, where $\hat{\mathbf{h}}_{\mathrm{E}}$ is the transmitter's erroneous estimate of $\mathbf{h}_{\mathrm{E}}$, and $\epsilon_{\mathbf{h}_{\mathrm{E}}}$ is some known constant. This model is well accepted to take into account channel uncertainty caused by limited feedback from the receiver [18, Lemma 1]. In wiretap scenarios, however, the spherical uncertainty model becomes inapplicable if the eavesdropper is a passive receiver and not part of the communication network.

In the remainder of this section, we declare the notation used throughout the paper. The system and channel models are described in Section II. In Section III, we consider the design of optimal and robust beamformers under the assumptions of perfect and imperfect channel information, respectively. In Section IV, we derive uncertainty sets for the eavesdropper's channel based on the uncertain parameters in the LoS channel gain equation. In Section V, we provide numerical examples to compare the performance of the proposed beamformers with conventional schemes. We also evaluate the worst-case secrecy rate performance in a typical VLC scenario. Finally, we provide our concluding remarks in Section VI.

Notation: The set of N-dimensional real-valued numbers is denoted by $\mathbb{R}^N$, and the set of N-dimensional nonnegative real-valued numbers is denoted by $\mathbb{R}_+^N$. Vectors are denoted by boldface lowercase letters, and matrices are denoted by boldface uppercase letters. We use $\mathbf{I}_N$ and $\mathbf{1}_N$ to denote the

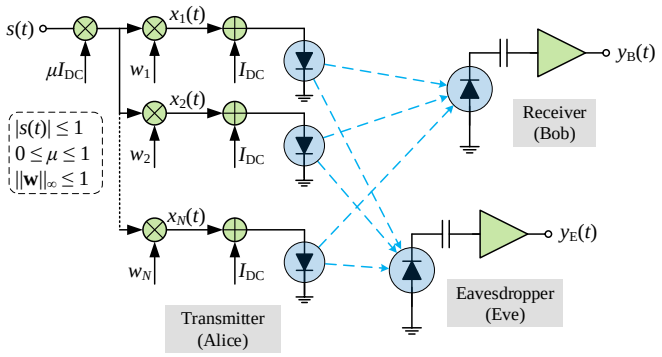

Fig. 1. A broadcast MISO VLC system with one intended receiver and one eavesdropper.

N-dimensional identity matrix and the all-one column vector of length N, respectively. We also use $\mathbf{Diag}(x_1, \ldots, x_N)$ to denote the diagonal matrix with diagonal elements $x_1, \ldots, x_N$. The absolute value is denoted by $|\cdot|$, and the l_p-norm, $p \geq 1$, is denoted by $\|\cdot\|_p$. The case $p = \infty$ designates the Chebyshev or l_∞-norm given by $\|\mathbf{x}\|_\infty = \max\{|x_1|, \ldots, |x_N|\}$. Transposition is denoted by the superscript $^{\mathrm{T}}$, and the Kronecker product is denoted by $\otimes$. We follow the convention in the physical-layer security literature and refer to the transmitter, legitimate receiver, and eavesdropper as *Alice*, *Bob*, and *Eve*, respectively. We use the subscripts $_{\mathrm{B}}$ and $_{\mathrm{E}}$ to denote relevance to Bob and Eve, respectively.

II. System and Channel Models

A. Problem Scenario

We consider secure downlink transmission in an indoor VLC link, in the presence of a passive eavesdropper, as illustrated in Figure 1. The service area, or simply the room, is illuminated by N_{Fix} lighting fixtures attached to the ceiling. Each fixture encloses N_{LED} high-brightness LEDs that can be modulated independently of each other using separate drivers. The total number of LEDs is $N = N_{\mathrm{Fix}} \times N_{\mathrm{LED}}$. In order to fulfill their primary role as luminaries, each LED is forward-biased by a fixed current I_{DC} to emit optical power $P_{\mathrm{opt}} = \eta I_{\mathrm{DC}}$, where η (W/A) is the current-to-optical-power conversion ratio. Information is relayed from the transmitter (Alice) to the legitimate receiver (Bob) by modulating the instantaneous optical output power of the LEDs. The eavesdropper (Eve) is a passive adversary attempting to intercept the connection between Alice and Bob.

B. Data Transmission

We consider a pulse-amplitude modulation system in which information symbols from a single-stream data source are stochastically encoded into a zero-mean current signal $s(t), t = 1, 2, \ldots$, where t is the time index. The codewords are drawn at random according to an independent and identically distributed (i.i.d.) uniform distribution over the interval $[-1, 1]$. Each codeword $s(t)$ is scaled by a constant μI_{DC}, where $\mu \in [0, 1]$ is termed as the *modulation index*. The modulation index is chosen such that the LED maintains linear current-to-optical-power conversion over the range $[(1-\mu)I_{\mathrm{DC}}, (1+\mu)I_{\mathrm{DC}}]$. If nonlinearity is severe, digital predistortion of the modulation current may be necessary to linearize the LED response around the DC bias point and increase the permissible dynamic range $2\mu I_{\mathrm{DC}}$ [19]. Then, the scaled codewords are multiplied by a fixed vector $\mathbf{w} \in \mathbb{R}^N$, $\|\mathbf{w}\|_\infty \leq 1$, referred to as the *beamformer*, resulting in the modulation current vector

$$\mathbf{x}(t) = \mu I_{\mathrm{DC}} \mathbf{w} s(t). \tag{1}$$

Thus, after adding the DC bias, the vector of instantaneous optical powers transmitted from the LEDs can be expressed as

$$\begin{aligned} \mathbf{P}_{\mathrm{Tx}}(t) &= \eta(I_{\mathrm{DC}}\mathbf{1}_N + \mathbf{x}(t)) \\ &= P_{\mathrm{opt}}(\mathbf{1}_N + \mu \mathbf{w} s(t)). \end{aligned} \tag{2}$$

In this work, we assume narrow-band transmission, i.e., the system bandwidth (e.g., 10 MHz [20]) is considerably smaller than the inverse of the maximum excess delay of the channel (about 10-20 nsec in a medium-sized room). Under this assumption, the frequency response of the VLC channel is almost flat near DC [21]. Therefore, it is sufficient to characterize the optical channel by its DC gain, which is the ratio of the transmitted to received optical powers. With multiple-LED transmission, the total received optical power, $P_{\mathrm{Rx}}(t)$, is the sum of optical powers collected from individual LEDs. Let $h_i \in \mathbb{R}_+$, $i = 1, \ldots, N$, denote the DC optical channel gain from the ith LED to the photodetector, then $P_{\mathrm{Rx}}(t)$ can be expressed as

$$\begin{aligned} P_{\mathrm{Rx}}(t) &= \mathbf{h}^{\mathrm{T}} \mathbf{P}_{\mathrm{Tx}}(t) \\ &= P_{\mathrm{opt}} \mathbf{h}^{\mathrm{T}} \mathbf{1}_N + \mu P_{\mathrm{opt}} \mathbf{h}^{\mathrm{T}} \mathbf{w} s(t), \end{aligned} \tag{3}$$

where $\mathbf{h} = [h_1 \ \ldots \ h_N]^{\mathrm{T}}$ is the DC optical channel gain vector. The first term on the right-hand side of (3) is the DC component that specifies the illumination level (or illuminance) perceived by the human eye at the receiver's location, whereas the second term is the data-signal component with zero mean. The optical power is converted by the receiver's photodetector into a proportional photocurrent, $RP_{\mathrm{Rx}}(t)$, corrupted by additive Gaussian noise, $n(t)$, where R (A/W) is the photodetector responsivity, and $n(t) \sim \mathcal{N}(0, \sigma^2)$.

Thus, after removing the DC components, the signals received by Bob and Eve, respectively, are given by

$$y_{\mathrm{B}}(t) = P \mathbf{h}_{\mathrm{B}}^{\mathrm{T}} \mathbf{w} s(t) + n_{\mathrm{B}}(t), \tag{4a}$$

$$y_{\mathrm{E}}(t) = P \mathbf{h}_{\mathrm{E}}^{\mathrm{T}} \mathbf{w} s(t) + n_{\mathrm{E}}(t), \tag{4b}$$

where $P \triangleq \mu P_{\mathrm{opt}} R$, $\mathbf{h}_{\mathrm{B}} \in \mathbb{R}_+^N$ and $\mathbf{h}_{\mathrm{E}} \in \mathbb{R}_+^N$ are Bob's and Eve's optical channel gain vectors, respectively, and $n_{\mathrm{B}} \sim \mathcal{N}(0, \sigma_{\mathrm{B}}^2)$ and $n_{\mathrm{E}} \sim \mathcal{N}(0, \sigma_{\mathrm{E}}^2)$ are Gaussian noises. For simplicity, and without loss of generality, we assume that $\sigma_{\mathrm{B}}^2 = \sigma_{\mathrm{E}}^2 = \sigma^2$. Equations (4a) and (4b) define a Gaussian MISO wiretap channel, and the input is subject to the amplitude constraint

$$\|\mathbf{w}\|_\infty \leq 1, \tag{5a}$$

$$|s(t)| \ \leq 1 \quad \forall t. \tag{5b}$$

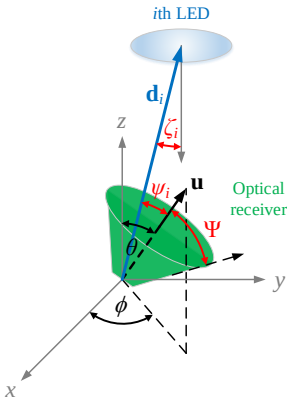

Fig. 2. Geometry of an LoS VLC link with arbitrary receiver orientation.

C. Optical Channel Gain

Figure 2 illustrates the geometry of an LoS VLC link. The receiver is pointing towards an arbitrary direction defined by the unit vector

$$\mathbf{u} = \begin{bmatrix} \sin\theta\cos\phi & \sin\theta\sin\phi & \cos\theta \end{bmatrix}^{\mathrm{T}},$$

where $\theta \in [0, \pi]$ is the zenith (or polar) angle, and $\phi \in [0, 2\pi]$ is the azimuth angle. We shall refer to $\mathbf{u}$ as the orientation vector.

We assume that the LEDs have an azimuth-symmetric generalized Lambertian emission pattern. We also assume that the LoS path is dominant over multipath components caused by diffuse reflections from nearby surfaces[1]. Under these assumptions, the DC optical channel gain h_i, $i = 1, \ldots, N$, can be accurately approximated by [21, Eq. (10)]

$$h_i = \frac{(m+1)A}{2\pi\|\mathbf{d}_i\|_2^2} (\cos\zeta_i)^m \, T_s \, g_{\mathrm{c}} \cos\psi_i \, I_\Psi(\psi_i) \tag{6a}$$

$$= \frac{(m+1)A}{2\pi\|\mathbf{d}_i\|_2^{m+3}} \, d_z^m \, T_s \, g_{\mathrm{c}} \, \mathbf{d}_i^{\mathrm{T}}\mathbf{u} \, I_\Psi\left(\cos^{-1}\frac{\mathbf{d}_i^{\mathrm{T}}\mathbf{u}}{\|\mathbf{d}_i\|_2}\right), \tag{6b}$$

where m is the Lambertian order, A is the area of the photodetector, $\mathbf{d}_i = [d_{x,i} \; d_{y,i} \; d_z]^{\mathrm{T}}$ is the displacement vector between the photodetector and the ith LED (see Figure 2), ζ_i is the angle of irradiance from the ith LED (measured with respect to the LED axis), T_s is the gain of the optical filter, g_{c} is the gain of the optical concentrator within its field-of-view (FoV), ψ_i is the angle of incidence from the ith LED (measured with respect to the receiver axis), and $I_\Psi(\cdot)$ is an indicator function defined as

$$I_\Psi(\psi) \triangleq \begin{cases} 1 & |\psi| \le \Psi \\ 0 & |\psi| > \Psi \end{cases},$$

where $\Psi \le \pi/2$ is the semi-angle FoV of the concentrator. Assuming an idealized non-imaging concentrator, g_{c} can be approximated by [21, Eq. (8)]

$$g_{\mathrm{c}} = \frac{n_{\mathrm{r}}^2}{\sin^2\Psi}, \tag{7}$$

where n_{r} is the refractive index of the concentrator material.

[1]This assumption will be relaxed in Section IV-D where the NLoS components are taken into account.

III. Optimal and Robust Beamformer Design

A. Performance Metric and Problem Formulation

A key performance metric of the wiretap channel is the *secrecy capacity* defined as the maximum communication rate at which Bob can reliably decode the transmitted message, while Eve cannot infer information at any positive rate [2]–[4]. The secrecy capacity of the Gaussian wiretap channel, subject to an *average power constraint*, is a well-studied problem, and it was shown that the maximizing input distribution is Gaussian, resulting in a closed-form secrecy capacity expression. On the other hand, with *amplitude constraints* on the channel input, the secrecy capacity is achieved by a discrete input distribution having a finite number of mass points [22]. For sufficiently-small amplitude constraints, the symmetric binary distribution has been shown to be optimal [22, Section IV]. For the general case, however, it is difficult to explicitly solve for the maximizing distribution, and thus the secrecy capacity can be only found via numerical methods. Since closed-form expressions are typically crucial for system design purposes, one might resort to upper and lower bounds on the secrecy capacity [7, Theorem 1].

Assuming uniform input distribution along with transmit beamforming, an achievable secrecy rate in $(\mathrm{bits/sec/Hz})$ for the Gaussian MISO wiretap channel (4), subject to the amplitude constraint in (5), is given by [7, Eq. (13)]

$$R_{\mathrm{s}} = \left[\frac{1}{2}\log_2\frac{6P^2(\mathbf{h}_{\mathrm{B}}^{\mathrm{T}}\mathbf{w})^2 + 3\pi e\sigma^2}{\pi e P^2(\mathbf{h}_{\mathrm{E}}^{\mathrm{T}}\mathbf{w})^2 + 3\pi e\sigma^2}\right]^+, \tag{8}$$

where $[x]^+ = \max\{x, 0\}$. A typical problem of interest is to find the optimal beamformer $\mathbf{w}^\star$ that maximizes the achievable secrecy rate, i.e.,

$$\mathbf{w}^\star = \underset{\|\mathbf{w}\|_\infty \le 1}{\operatorname{argmax}} \; R_{\mathrm{s}}. \tag{9}$$

In fact, our main goal in this paper is to solve the design problem in (9). To this end, we have to overcome two major difficulties. Firstly, the problem in (9) is clearly nonconvex, and the amplitude constraint on the beamformer $\mathbf{w}$ makes it different from the well-known *Rayleigh quotient* maximization problem. In the next subsection, we introduce Proposition 1 to transform this nonconvex problem into a solvable quasiconvex line search problem. Secondly, it is unrealistic in most practical cases to assume that the channel gain vectors $\mathbf{h}_{\mathrm{B}}$ and $\mathbf{h}_{\mathrm{E}}$ are precisely known to Alice. On one hand, information regarding Bob's channel might suffer from estimation errors, aside from inevitable quantization errors imposed by the finite rate of the feedback channel. On the other hand, there might be no feedback from Eve regarding her channel if Eve is a passive eavesdropper and shall remain silent to hide her presence. In this case, Alice must resort to less reliable information sources, such as Eve's location and orientation, in order to obtain an estimate of her channel gain. In all cases, solving (9) for some uncertain estimates of $\mathbf{h}_{\mathrm{B}}$ and $\mathbf{h}_{\mathrm{E}}$ can be meaningless as secrecy outage will occur if the actual realizations of $\mathbf{h}_{\mathrm{B}}$ and $\mathbf{h}_{\mathrm{E}}$ significantly deviate from their nominal values. Therefore, a more appropriate design approach is to devise reasonable uncertainty sets, $\mathcal{H}_{\mathrm{B}}$ and $\mathcal{H}_{\mathrm{E}}$, that enclose all

possible realizations of $\mathbf{h}_{\mathrm{B}}$ and $\mathbf{h}_{\mathrm{E}}$, respectively, in a given scenario, and solve the *robust counterpart* [23] of (9) to maximize the secrecy rate corresponding to the worst-case realization of $(\mathbf{h}_{\mathrm{B}}, \mathbf{h}_{\mathrm{E}}) \in \mathcal{H}_{\mathrm{B}} \times \mathcal{H}_{\mathrm{E}}$. That is to solve

$$\underset{\|\mathbf{w}\|_\infty \leq 1}{\text{maximize}} \; R_{\mathrm{s}} \quad \forall (\mathbf{h}_{\mathrm{B}}, \mathbf{h}_{\mathrm{E}}) \in \mathcal{H}_{\mathrm{B}} \times \mathcal{H}_{\mathrm{E}}, \tag{10a}$$

or, equivalently,

$$\underset{\|\mathbf{w}\|_\infty \leq 1}{\text{maximize}} \; \min_{\substack{\mathbf{h}_{\mathrm{B}} \in \mathcal{H}_{\mathrm{B}} \\ \mathbf{h}_{\mathrm{E}} \in \mathcal{H}_{\mathrm{E}}}} R_{\mathrm{s}}. \tag{10b}$$

The robust design problem in (10) will be tackled in Section III-C via Proposition 2, whereas in Section IV, we discuss methods to model uncertainty in Eve's channel, in VLC scenarios, without feedback from Eve.

B. Optimal Beamforming with Perfect Channel Information

Our focus in this subsection is on solving the design problem in (9) under the premise of perfect channel information. Although the constraint on the beamformer is specified by $\|\mathbf{w}\|_\infty \leq 1$, i.e., an amplitude or l_∞-norm constraint, we shall in fact solve the problem subject to a general l_p-norm constraint, i.e., for any $p \geq 1$.

Proposition 1: (Certain $\mathbf{h}_{\mathrm{B}}$ and $\mathbf{h}_{\mathrm{E}}$) Let $\|\mathbf{w}\|_p$, $p \geq 1$, denote the l_p-norm of $\mathbf{w}$, then the maximization problem

$$\underset{\|\mathbf{w}\|_p \leq 1}{\text{maximize}} \; \frac{6P^2(\mathbf{h}_{\mathrm{B}}^{\mathrm{T}}\mathbf{w})^2 + 3\pi e\sigma^2}{\pi e P^2(\mathbf{h}_{\mathrm{E}}^{\mathrm{T}}\mathbf{w})^2 + 3\pi e\sigma^2} \tag{11}$$

is equivalent to the quasiconvex problem (or quasiconcave maximization problem)

$$\underset{\alpha \in [\alpha_{\min}, \sqrt{6/\pi e}]}{\text{maximize}} \; \frac{6P^2(\mathbf{h}_{\mathrm{B}}^{\mathrm{T}}\mathbf{w}_\alpha)^2 + 3\pi e\sigma^2}{\pi e\alpha^2 P^2(\mathbf{h}_{\mathrm{B}}^{\mathrm{T}}\mathbf{w}_\alpha)^2 + 3\pi e\sigma^2}, \tag{12}$$

where $\alpha_{\min}$, the lower bound on α, is obtained by

$$\alpha_{\min} = \min_{\mathbf{w},\alpha} \; \alpha \tag{13a}$$

$$\text{s.t.} \;\; \mathbf{h}_{\mathrm{B}}^{\mathrm{T}}\mathbf{w} = 1, \tag{13b}$$

$$|\mathbf{h}_{\mathrm{E}}^{\mathrm{T}}\mathbf{w}| \leq \alpha, \tag{13c}$$

and, for each $\alpha \in [\alpha_{\min}, \sqrt{6/\pi e}]$, $\mathbf{w}_\alpha$ is obtained by

$$\mathbf{w}_\alpha = \underset{\|\mathbf{w}\|_p \leq 1}{\text{argmax}} \; \mathbf{h}_{\mathrm{B}}^{\mathrm{T}}\mathbf{w} \tag{14a}$$

$$\text{s.t.} \;\; |\mathbf{h}_{\mathrm{E}}^{\mathrm{T}}\mathbf{w}| \leq \alpha \mathbf{h}_{\mathrm{B}}^{\mathrm{T}}\mathbf{w}. \tag{14b}$$

Proof: Please refer to Appendix A. ∎

Remarks:

- Proposition 1 has a practical interpretation. It reveals that the achievable secrecy rate is a quasiconcave function of the parameter α, which is the ratio of the signal level at Eve to the signal level at Bob[2]. This is provably true for an arbitrary l_p-norm constraint on $\mathbf{w}$, i.e., for any $p \geq 1$.
- Setting $\alpha = 0$ in (14) corresponds to the zero-forcing (ZF) beamforming case, i.e., $\mathbf{w}_{\alpha=0}$ is the best ZF beamformer.
- If $N \geq 2$, and $\mathbf{h}_{\mathrm{B}}$ and $\mathbf{h}_{\mathrm{E}}$ are linearly independent, then $\alpha_{\min} = 0$ and ZF is feasible.

Proposition 1 involves two optimization problems. The outer problem (12) is a quasiconvex line search problem whose globally optimal solution can be found by performing a bisection search on $\alpha \in [\alpha_{\min}, \sqrt{6/\pi e}]$, on a logarithmic scale. In the next subsection, we propose Algorithm 1 to solve (12), as well as the corresponding problem in the more general case of uncertain channel information. In each iteration of the bisection search, the inner problem (14) should be solved to obtain $\mathbf{w}_\alpha$ and calculate the objective function in (12). Problem (14) is convex for any $p \geq 1$, and can be efficiently solved in a polynomial time.

Using (12), the achievable secrecy rate, as a function of α, is given by

$$R_{\mathrm{s}}(\alpha) = \left[\frac{1}{2}\log_2 \frac{6P^2(\mathbf{h}_{\mathrm{B}}^{\mathrm{T}}\mathbf{w}_\alpha)^2 + 3\pi e\sigma^2}{\pi e\alpha^2 P^2(\mathbf{h}_{\mathrm{B}}^{\mathrm{T}}\mathbf{w}_\alpha)^2 + 3\pi e\sigma^2}\right]^+. \tag{15}$$

Let $\alpha^\star$ denote the global maximizer of (12), then the optimal beamformer $\mathbf{w}^\star$ is the solution of (14) corresponding to $\alpha = \alpha^\star$, i.e., $\mathbf{w}^\star \equiv \mathbf{w}_{\alpha^\star}$, and the maximum achievable secrecy rate is equal to $R_{\mathrm{s}}(\alpha^\star)$.

C. Robust Beamforming with Imperfect Channel Information

In this subsection, we extend the approach we used in Proposition 1 to take into account uncertainty in channel information for both Bob and Eve.

Proposition 2: (Uncertain $\mathbf{h}_{\mathrm{B}}$ and $\mathbf{h}_{\mathrm{E}}$) Given a convex set $\mathcal{H}_{\mathrm{B}}$ and an arbitrary set $\mathcal{H}_{\mathrm{E}}$, the max-min problem

$$\underset{\|\mathbf{w}\|_p \leq 1}{\text{maximize}} \; \min_{\substack{\mathbf{h}_{\mathrm{B}} \in \mathcal{H}_{\mathrm{B}} \\ \mathbf{h}_{\mathrm{E}} \in \mathcal{H}_{\mathrm{E}}}} \frac{6P^2(\mathbf{h}_{\mathrm{B}}^{\mathrm{T}}\mathbf{w})^2 + 3\pi e\sigma^2}{\pi e P^2(\mathbf{h}_{\mathrm{E}}^{\mathrm{T}}\mathbf{w})^2 + 3\pi e\sigma^2}, \tag{16}$$

for any $p \geq 1$, is equivalent to the quasiconvex problem

$$\underset{\alpha \in [\alpha_{\min}, \sqrt{6/\pi e}]}{\text{maximize}} \; \frac{6P^2 t_\alpha^2 + 3\pi e\sigma^2}{\pi e\alpha^2 P^2 t_\alpha^2 + 3\pi e\sigma^2}, \tag{17}$$

where $\alpha_{\min}$ is obtained by

$$\alpha_{\min} = \min_{\mathbf{w},\alpha} \; \alpha \tag{18a}$$

$$\text{s.t.} \;\; \mathbf{h}_{\mathrm{B}}^{\mathrm{T}}\mathbf{w} \geq 1 \quad \forall \mathbf{h}_{\mathrm{B}} \in \mathcal{H}_{\mathrm{B}}, \tag{18b}$$

$$|\mathbf{h}_{\mathrm{E}}^{\mathrm{T}}\mathbf{w}| \leq \alpha \quad \forall \mathbf{h}_{\mathrm{E}} \in \mathcal{H}_{\mathrm{E}}, \tag{18c}$$

and, for each $\alpha \in [\alpha_{\min}, \sqrt{6/\pi e}]$, t_α is obtained from

$$(\mathbf{w}_\alpha, t_\alpha) = \underset{\|\mathbf{w}\|_p \leq 1, t}{\text{argmax}} \; t \tag{19a}$$

$$\text{s.t.} \;\; \mathbf{h}_{\mathrm{B}}^{\mathrm{T}}\mathbf{w} \geq t \quad \forall \mathbf{h}_{\mathrm{B}} \in \mathcal{H}_{\mathrm{B}}, \tag{19b}$$

$$|\mathbf{h}_{\mathrm{E}}^{\mathrm{T}}\mathbf{w}| \leq \alpha t \quad \forall \mathbf{h}_{\mathrm{E}} \in \mathcal{H}_{\mathrm{E}}. \tag{19c}$$

Proof: Please refer to Appendix B. ∎

Remarks:

- $\alpha_{\min} > 0$ implies that ZF is not feasible.

[2]Recall from (4) that, without loss of generality, we assume equal noise variance at Bob and Eve.

- $\alpha_{\min} \geq \sqrt{6/\pi e}$ implies that the max-min problem is not feasible and the worst-case secrecy rate is zero (e.g., when $\mathcal{H}_{\mathrm{B}} \cap \mathcal{H}_{\mathrm{E}} \neq \emptyset$).

Similar to (12) in Proposition 1, the outer problem (17) is quasiconvex and can be efficiently solved by performing a bisection search on α. We propose the following iterative algorithm to obtain a solution $\alpha^\star$ with accuracy ϵ_α (dB).

Algorithm 1 Bisection search to solve (17) in Proposition 2

1: Solve (18) to obtain $\alpha_{\min}$
2: **if** $\alpha_{\min} < 10^{-10}$, **then** $\alpha_{\min} := 10^{-10}$
3: Initialize $\overline{\alpha} = 20\log_{10}\sqrt{6/\pi e}$ and $\underline{\alpha} = 20\log_{10}\alpha_{\min}$
4: **given** the required accuracy ϵ_α (dB), set the positive constant Δ_α such that $0 < 20\log_{10}\Delta_\alpha < \epsilon_\alpha$
5: **while** $\overline{\alpha} - \underline{\alpha} \geq \epsilon_\alpha$ **do**
6: $\quad \alpha_{(\mathrm{dB})} := (\overline{\alpha} + \underline{\alpha})/2$
7: $\quad$ Solve (19) with α to obtain t_α, where $\alpha = 10^{\frac{\alpha_{(\mathrm{dB})}}{20}}$
8: $\quad$ Calculate the objective in (17), $f(\alpha) = \frac{6P^2t_\alpha^2 + 3\pi e\sigma^2}{\pi e\alpha^2P^2t_\alpha^2 + 3\pi e\sigma^2}$
9: $\quad$ Solve (19) with $\alpha + \Delta_\alpha$ to obtain $t_{\alpha+\Delta_\alpha}$
10: $\quad$ Calculate $f(\alpha+\Delta_\alpha) = \frac{6P^2t_{\alpha+\Delta_\alpha}^2 + 3\pi e\sigma^2}{\pi e(\alpha+\Delta_\alpha)^2P^2t_{\alpha+\Delta_\alpha}^2 + 3\pi e\sigma^2}$
11: $\quad$ **if** $f(\alpha+\Delta_\alpha) - f(\alpha) > 0$, **then** $\underline{\alpha} := \alpha_{(\mathrm{dB})}$ **else** $\overline{\alpha} := \alpha_{(\mathrm{dB})}$
12: **end while**
13: **return** $\alpha^\star := \alpha$

Assuming $\epsilon_\alpha = 0.2$ dB, Algorithm 1 shall converge in at most $\lceil \log_2(20\log_{10}\frac{\sqrt{6/\pi e}}{10^{-10}}) - \log_2\epsilon_\alpha \rceil = 10$ iterations [24, Section 4.2.5]. Note, however, that the inner problem (19) should be solved twice in each iteration. Thus, although Proposition 2 is valid in principle for any convex set $\mathcal{H}_{\mathrm{B}}$ and an arbitrary set $\mathcal{H}_{\mathrm{E}}$, it is practically useful only when (19) is tractable, i.e., can be efficiently solved. Problem (19) is a *robust convex program* whose tractability depends solely on the geometries of $\mathcal{H}_{\mathrm{B}}$ and $\mathcal{H}_{\mathrm{E}}$ [23], [25], [26]. In Section IV, we use a spherical set $\mathcal{H}_{\mathrm{B}}$ to accommodate quantization errors caused by limited feedback from Bob. For Eve's channel, we use discrete, interval, and ellipsoidal sets to model different uncertainty sources that cause inaccurate estimates of $\mathbf{h}_{\mathrm{E}}$ in VLC scenarios. Using a spherical set $\mathcal{H}_{\mathrm{B}}$, and discrete, interval, or ellipsoidal sets $\mathcal{H}_{\mathrm{E}}$, and assuming that $p \in \{1, 2, \infty\}$[3], the inner problem (19) can be expressed as a second-order cone problem. The ϵ-accurate solution of such a problem can be found using interior-point methods in $\mathcal{O}(\sqrt{N}\log(1/\epsilon))$ iterations [28], for any $\epsilon > 0$.

From (17), the worst-case secrecy rate, as a function of α, is given by

$$R_{\mathrm{s}}^{\mathrm{wc}}(\alpha) = \left[\frac{1}{2}\log_2\frac{6P^2t_\alpha^2 + 3\pi e\sigma^2}{\pi e\alpha^2P^2t_\alpha^2 + 3\pi e\sigma^2}\right]^+. \tag{20}$$

The best worst-case secrecy rate is equal to $R_{\mathrm{s}}^{\mathrm{wc}}(\alpha^\star)$ and is achieved by the robust beamformer $\mathbf{w}_{\alpha^\star}$.

IV. Uncertainty Sets for the Eavesdropper's Channel in VLC Scenarios

Our focus in this section is on deriving uncertainty sets for Eve's channel based on the uncertain parameters in the LoS channel gain equation in (6). Our motivation towards this approach is the lack of feedback from Eve regarding her channel when Eve is a passive or non-cooperative receiver. In particular, we take advantage of the fact that $\mathbf{h}_{\mathrm{E}}$ can be predicted from Eve's location and orientation using (6) if the LoS path is dominant and the emission pattern of the LEDs is known. Such information can be mapped into an estimate of $\mathbf{h}_{\mathrm{E}}$ surrounded by a reasonable uncertainty set $\mathcal{H}_{\mathrm{E}}$. Unfortunately, the channel gain expression in (6) is quite complex, and mapping such uncertain parameters altogether into a useful $\mathcal{H}_{\mathrm{E}}$ that makes (19) solvable is quite difficult. Thus, we begin with studying uncertainty sets corresponding to one uncertain parameter at a time. We also consider uncertainty caused by the NLoS components in $\mathbf{h}_{\mathrm{E}}$. Cases involving more than one uncertainty source will also be briefly discussed.

Throughout the entire section, we assume an amplitude constraint on $\mathbf{w}$, i.e., $\|\mathbf{w}\|_\infty \leq 1$. Furthermore, we assume spherical uncertainty for Bob's channel, i.e., $\mathbf{h}_{\mathrm{B}} \in \mathcal{H}_{\mathrm{B}}$,

$$\mathcal{H}_{\mathrm{B}} = \left\{\hat{\mathbf{h}}_{\mathrm{B}} + \mathbf{e}_{\mathbf{h}_{\mathrm{B}}} : \|\mathbf{e}_{\mathbf{h}_{\mathrm{B}}}\|_2 \leq \epsilon_{\mathbf{h}_{\mathrm{B}}}\right\}, \tag{21}$$

where the nominal vector $\hat{\mathbf{h}}_{\mathrm{B}}$ is known to Alice via limited feedback from Bob, and the bounded error term $\mathbf{e}_{\mathbf{h}_{\mathrm{B}}}$ is due to quantization errors. Substituting (21) back into (19b), the latter can be expressed as

$$\hat{\mathbf{h}}_{\mathrm{B}}^{\mathrm{T}}\mathbf{w} - \epsilon_{\mathbf{h}_{\mathrm{B}}}\|\mathbf{w}\|_2 \geq t. \tag{22}$$

A. Uncertain Eavesdropper's Location

In this subsection, we consider uncertainty caused by inaccurate information regarding Eve's location. We assume that Eve is located inside a three-dimensional rectangular region (or box) $\mathcal{B}$ with dimensions $(2l_x, 2l_y, 2l_z)$. We also assume, without loss of generality, that $\mathcal{B}$ is centered at the origin, i.e.,

$$\mathcal{B} = \left\{\mathbf{L}\boldsymbol{v} : \boldsymbol{v} \in \mathbb{R}^3, \|\boldsymbol{v}\|_\infty \leq 1\right\}, \tag{23}$$

where $\mathbf{L} \triangleq \mathbf{Diag}(l_x, l_y, l_z)$. Furthermore, we choose the origin (or the enter of $\mathcal{B}$) as the nominal location of Eve.

Let $\boldsymbol{\delta} = [\delta_x \ \delta_y \ \delta_z]^{\mathrm{T}}$, $\boldsymbol{\delta} \in \mathcal{B}$, denote the deviation of the actual location of Eve from the origin. Then, the optical channel gain h_i, $i = 1, \ldots, N$, anywhere inside $\mathcal{B}$, as a function of $\boldsymbol{\delta}$, is given by

$$h_i(\boldsymbol{\delta}) = \frac{(m+1)A}{2\pi\|\mathbf{d}_i - \boldsymbol{\delta}\|_2^{m+3}}(d_z - \delta_z)^m T_s\, g_{\mathrm{c}}\,(\mathbf{d}_i - \boldsymbol{\delta})^{\mathrm{T}}\mathbf{u} \times I_{\Psi_{\mathrm{E}}}\left(\cos^{-1}\frac{(\mathbf{d}_i - \boldsymbol{\delta})^{\mathrm{T}}\mathbf{u}}{\|\mathbf{d}_i - \boldsymbol{\delta}\|_2}\right), \tag{24}$$

and the set of all possible channel realizations inside $\mathcal{B}$ can be written as

$$\mathcal{H}_{\mathrm{E}}^{\mathcal{B}} = \{\mathbf{h}(\boldsymbol{\delta}) : \boldsymbol{\delta} \in \mathcal{B}\}. \tag{25}$$

If we substitute with $\mathcal{H}_{\mathrm{E}} = \mathcal{H}_{\mathrm{E}}^{\mathcal{B}}$ back into (19c), we will end up with an intractable semi-infinite optimization problem. Therefore, we shall discuss methods to approximate $\mathcal{H}_{\mathrm{E}}^{\mathcal{B}}$, based on the volume of $\mathcal{B}$, in order to make (19) solvable.

[3]We need the assumption $p \in \{1, 2, \infty\}$ merely to state that the resulting problem is a second-order cone for which complexity is known to be $\mathcal{O}(\sqrt{N}\log(1/\epsilon))$. However, the problem is still convex and equally solvable, e.g., via the CVX toolbox [27], for any $p \geq 1$.

1) Small uncertainty region: For sufficiently-small $\mathcal{B}$, e.g., $\max\{2l_x, 2l_y, 2l_z\} \leq 0.5$ m, we can assume that the subset of LEDs seen by Eve's receiver at a particular location $\boldsymbol{\delta}$,

$$\mathcal{I}_{\boldsymbol{\delta}} = \left\{ i : I_{\Psi_{\mathrm{E}}}\left(\cos^{-1} \frac{(\mathbf{d}_i - \boldsymbol{\delta})^{\mathrm{T}} \mathbf{u}}{\|\mathbf{d}_i - \boldsymbol{\delta}\|_2} \right) = 1,\ i \in \{1, \ldots, N\} \right\},$$

is identical for all $\boldsymbol{\delta} \in \mathcal{B}$. In other words, the output of the indicator function in (24) is independent of $\boldsymbol{\delta}$ for all the LEDs and is solely determined by the nominal location of Eve. Under this assumption, the channel gain (24) can be written as

$$h_i(\boldsymbol{\delta}) = c_i \, \frac{(d_z - \delta_z)^m (\mathbf{d}_i - \boldsymbol{\delta})^{\mathrm{T}} \mathbf{u}}{\|\mathbf{d}_i - \boldsymbol{\delta}\|_2^{m+3}}, \tag{26}$$

where

$$c_i \triangleq \frac{(m+1)A}{2\pi} \, T_s \, g_{\mathrm{c}} \, I_{\Psi_{\mathrm{E}}}\left(\cos^{-1} \frac{\mathbf{d}_i^{\mathrm{T}} \mathbf{u}}{\|\mathbf{d}_i\|_2} \right). \tag{27}$$

Furthermore, with sufficiently small $\mathcal{B}$, $\mathbf{h}(\boldsymbol{\delta})$ can be well approximated by its first-order approximation around the center of $\mathcal{B}$, that is

$$\mathbf{h}(\boldsymbol{\delta}) \approx \bar{\mathbf{h}}(\boldsymbol{\delta}) = \mathbf{h_0} + \mathbf{J_0}\boldsymbol{\delta}, \tag{28}$$

where $\mathbf{h_0} \equiv \mathbf{h}(\mathbf{0})$, $\mathbf{J} \in \mathbb{R}^{N \times 3}$ is the *Jacobian matrix* (or matrix of partial derivatives), defined as

$$\mathbf{J} \triangleq \begin{bmatrix} \frac{\partial h_1(\boldsymbol{\delta})}{\partial \delta_x} & \frac{\partial h_1(\boldsymbol{\delta})}{\partial \delta_y} & \frac{\partial h_1(\boldsymbol{\delta})}{\partial \delta_z} \\ \vdots & \vdots & \vdots \\ \frac{\partial h_N(\boldsymbol{\delta})}{\partial \delta_x} & \frac{\partial h_N(\boldsymbol{\delta})}{\partial \delta_y} & \frac{\partial h_N(\boldsymbol{\delta})}{\partial \delta_z} \end{bmatrix}, \tag{29}$$

and $\mathbf{J_0} \equiv \mathbf{J}(\mathbf{0})$. The entries of $\mathbf{h_0}$ and $\mathbf{J_0}$ are provided in Appendix D. Using the linearized channel gain expression in (28), the uncertainty set $\mathcal{H}_{\mathrm{E}}^{\mathcal{B}}$ can be approximated by

$$\bar{\mathcal{H}}_{\mathrm{E}}^{\mathcal{B}} = \left\{ \mathbf{h_0} + \mathbf{J_0}\mathbf{L}\boldsymbol{v} : \boldsymbol{v} \in \mathbb{R}^3, \|\boldsymbol{v}\|_\infty \leq 1 \right\}. \tag{30}$$

Substituting with $\bar{\mathcal{H}}_{\mathrm{E}}^{\mathcal{B}}$ back into (19c), the problem in (19) can be expressed as

$$\begin{aligned} \underset{\|\mathbf{w}\|_\infty \leq 1, t}{\text{maximize}} \quad & t && \text{(31a)} \\ \text{s.t.} \quad & \hat{\mathbf{h}}_{\mathrm{B}}^{\mathrm{T}} \mathbf{w} - \epsilon_{\mathbf{h}_{\mathrm{B}}} \|\mathbf{w}\|_2 \geq t, && \text{(31b)} \\ & |\mathbf{h_0}^{\mathrm{T}} \mathbf{w} + \boldsymbol{v}^{\mathrm{T}} \mathbf{L} \mathbf{J_0}^{\mathrm{T}} \mathbf{w}| \leq \alpha t \quad \forall \boldsymbol{v} : \|\boldsymbol{v}\|_\infty \leq 1, && \text{(31c)} \end{aligned}$$

or, equivalently,

$$\begin{aligned} \underset{\|\mathbf{w}\|_\infty \leq 1, t}{\text{maximize}} \quad & t && \text{(32a)} \\ \text{s.t.} \quad & \hat{\mathbf{h}}_{\mathrm{B}}^{\mathrm{T}} \mathbf{w} - \epsilon_{\mathbf{h}_{\mathrm{B}}} \|\mathbf{w}\|_2 \geq t, && \text{(32b)} \\ & \mathbf{h_0}^{\mathrm{T}} \mathbf{w} + \|\mathbf{L}\mathbf{J_0}^{\mathrm{T}} \mathbf{w}\|_1 \leq \alpha t, && \text{(32c)} \\ & \mathbf{h_0}^{\mathrm{T}} \mathbf{w} - \|\mathbf{L}\mathbf{J_0}^{\mathrm{T}} \mathbf{w}\|_1 \geq -\alpha t, && \text{(32d)} \end{aligned}$$

which is a second-order cone problem. Similarly, the problem in (18) can be expressed as

$$\begin{aligned} \underset{\mathbf{w}, \alpha}{\text{minimize}} \quad & \alpha && \text{(33a)} \\ \text{s.t.} \quad & \hat{\mathbf{h}}_{\mathrm{B}}^{\mathrm{T}} \mathbf{w} - \epsilon_{\mathbf{h}_{\mathrm{B}}} \|\mathbf{w}\|_2 \geq 1, && \text{(33b)} \\ & \mathbf{h_0}^{\mathrm{T}} \mathbf{w} + \|\mathbf{L}\mathbf{J_0}^{\mathrm{T}} \mathbf{w}\|_1 \leq \alpha, && \text{(33c)} \\ & \mathbf{h_0}^{\mathrm{T}} \mathbf{w} - \|\mathbf{L}\mathbf{J_0}^{\mathrm{T}} \mathbf{w}\|_1 \geq -\alpha. && \text{(33d)} \end{aligned}$$

2) Large uncertainty region: If the uncertainty region $\mathcal{B}$ is relatively large, the first-order approximation in (28) may become poor. Nevertheless, $\mathcal{B}$ can be first divided into K non-overlapping boxes, $\mathcal{B}_k$, $k = 1, \ldots, K$, such that $\bigcup_{k=1}^{K} \mathcal{B}_k = \mathcal{B}$. Then, the first-order approximation is performed inside each box, around its center, and (31) is solved with the corresponding K constraints.

Alternatively, the region $\mathcal{B}$ can be discretized using a three-dimensional fine grid $\ddot{\mathcal{B}}$, and the problem in (19) is approximated by

$$\begin{aligned} \underset{\|\mathbf{w}\|_\infty \leq 1, t}{\text{maximize}} \quad & t && \text{(34a)} \\ \text{s.t.} \quad & \hat{\mathbf{h}}_{\mathrm{B}}^{\mathrm{T}} \mathbf{w} - \epsilon_{\mathbf{h}_{\mathrm{B}}} \|\mathbf{w}\|_2 \geq t, && \text{(34b)} \\ & |\mathbf{h}^{\mathrm{T}}(\boldsymbol{\delta})\, \mathbf{w}| \leq \alpha t \quad \forall \boldsymbol{\delta} \in \ddot{\mathcal{B}}, && \text{(34c)} \end{aligned}$$

where the entries of $\mathbf{h}(\boldsymbol{\delta})$ are obtained with (24). Although discretization is a straightforward approach that results in linear constraints, the number of constraints may grow up very quickly with large uncertainty regions.

B. Uncertain Eavesdropper's Orientation

In this subsection, we assume that Eve has the freedom to adjust the direction of her receiver, $(\theta_{\mathrm{E}}, \phi_{\mathrm{E}})$, $\theta_{\mathrm{E}} \in [\theta_{\min}, \theta_{\max}]$, $\phi_{\mathrm{E}} \in [\phi_{\min}, \phi_{\max}]$, to her advantage. In other words, the exact direction of Eve's receiver is unknown to Alice. The uncertainty set $\mathcal{U}$ containing all possible realizations of Eve's orientation vector $\mathbf{u}$ can be written as

$$\mathcal{U} = \left\{ \mathbf{u} = \begin{bmatrix} \sin\theta\cos\phi \\ \sin\theta\sin\phi \\ \cos\theta \end{bmatrix} : \begin{array}{c} \theta \in [\theta_{\min}, \theta_{\max}], \\ \phi \in [\phi_{\min}, \phi_{\max}] \end{array} \right\}, \tag{35}$$

and the optical channel gain h_i, $i = 1, \ldots, N$, as a function of $\mathbf{u}$, is given by

$$h_i(\mathbf{u}) = c_i \frac{d_z^m}{\|\mathbf{d}_i\|_2^{m+3}} \mathbf{d}_i^{\mathrm{T}} \mathbf{u}, \tag{36}$$

where c_i is as defined in (27). Let $\mathbf{D} \in \mathbb{R}^{N \times 3}$ be defined as

$$\mathbf{D} \triangleq d_z^m \begin{bmatrix} \frac{c_1 \mathbf{d}_1}{\|\mathbf{d}_1\|_2^{m+3}} & \cdots & \frac{c_N \mathbf{d}_N}{\|\mathbf{d}_N\|_2^{m+3}} \end{bmatrix}^{\mathrm{T}}. \tag{37}$$

Then, $\mathbf{h}(\mathbf{u})$ can be expressed as

$$\mathbf{h}(\mathbf{u}) = \mathbf{D}\mathbf{u}. \tag{38}$$

Note from (27) and (37) that $\mathbf{D}$ depends on $\mathbf{u}$ via the indicator function in the definition of c_i, $i = 1, \ldots, N$. Thus, in general, $\mathbf{h}$ is not a linear function of $\mathbf{u}$. The set of all possible channel gains for Eve is given by

$$\mathcal{H}_{\mathrm{E}}^{\mathcal{U}} = \{\mathbf{D}\mathbf{u} : \mathbf{u} \in \mathcal{U}\}. \tag{39}$$

Substituting with $\mathcal{H}_{\mathrm{E}}^{\mathcal{U}}$ back into (19c), the problem in (19) can be written as

$$\begin{aligned} \underset{\|\mathbf{w}\|_\infty \leq 1, t}{\text{maximize}} \quad & t && \text{(40a)} \\ \text{s.t.} \quad & \hat{\mathbf{h}}_{\mathrm{B}}^{\mathrm{T}} \mathbf{w} - \epsilon_{\mathbf{h}_{\mathrm{B}}} \|\mathbf{w}\|_2 \geq t, && \text{(40b)} \\ & \max_{\mathbf{u} \in \mathcal{U}} |\mathbf{u}^{\mathrm{T}} \mathbf{D}^{\mathrm{T}} \mathbf{w}| \leq \alpha t. && \text{(40c)} \end{aligned}$$

In order to efficiently solve (40), we shall differentiate between two cases, as follows.

1) Small angle variations: In this case, we assume that Eve's freedom to adjust her receiver's orientation is limited in the sense that the subset of LEDs inside Eve's FoV at a particular direction $\mathbf{u}$,

$$\mathcal{I}_{\mathbf{u}} = \left\{ i : I_{\Psi_{\mathrm{E}}} \left(\cos^{-1} \frac{\mathbf{d}_i^{\mathrm{T}} \mathbf{u}}{\|\mathbf{d}_i\|_2} \right) = 1,\, i \in \{1, \ldots, N\} \right\},$$

remains unchanged for all $\mathbf{u} \in \mathcal{U}$. Perhaps the most practical case in which the above assumption may hold is when the permissible variations of the zenith angle θ_{E} is relatively small and close to zero, i.e., $\theta_{\mathrm{E}} \in [0, \theta_{\max}]$, where $\theta_{\max}$ is relatively small (e.g., $\theta_{\max} \leq 30^\circ$). If $\mathcal{I}_{\mathbf{u}}$ is fixed for all $\mathbf{u} \in \mathcal{U}$, then $\mathbf{D}$ is independent of $\mathbf{u}$, and $\mathbf{h}$, as given in (38), is a linear function of $\mathbf{u}$. In this case, the left-hand side of the inequality in (40c) can be upper-bounded as

$$\max_{\mathbf{u} \in \mathcal{U}} |\mathbf{u}^{\mathrm{T}} \mathbf{D}^{\mathrm{T}} \mathbf{w}| \leq \max_{\|\mathbf{u}\|_2 \leq 1} \mathbf{u}^{\mathrm{T}} \mathbf{D}^{\mathrm{T}} \mathbf{w} = \|\mathbf{D}^{\mathrm{T}} \mathbf{w}\|_2. \tag{41}$$

Then, the problem in (40) is replaced by

$$\begin{aligned} \underset{\|\mathbf{w}\|_\infty \leq 1, t}{\text{maximize}} \quad & t && \text{(42a)} \\ \text{s.t.} \quad & \hat{\mathbf{h}}_{\mathrm{B}}^{\mathrm{T}} \mathbf{w} - \epsilon_{\mathbf{h}_{\mathrm{B}}} \|\mathbf{w}\|_2 \geq t, && \text{(42b)} \\ & \|\mathbf{D}^{\mathrm{T}} \mathbf{w}\|_2 \leq \alpha t, && \text{(42c)} \end{aligned}$$

which is a second-order cone problem.

2) Large angle variations: With arbitrary zenith and/or azimuth angle variations for Eve's receiver, $\mathbf{D}$ becomes dependent on $\mathbf{u}$, and linearity between $\mathbf{h}$ and $\mathbf{u}$ is no longer maintained. In this case, it becomes difficult to obtain a mathematically-convenient uncertainty set $\mathcal{H}_{\mathrm{E}}^{\mathcal{U}}$ over the continuum of θ_{E} and ϕ_{E}. Thus, we resort to sampling $\mathbf{h}(\mathbf{u})$ over $\mathcal{U}$, and the inner problem (19) is approximated by

$$\begin{aligned} \underset{\|\mathbf{w}\|_\infty \leq 1, t}{\text{maximize}} \quad & t && \text{(43a)} \\ \text{s.t.} \quad & \hat{\mathbf{h}}_{\mathrm{B}}^{\mathrm{T}} \mathbf{w} - \epsilon_{\mathbf{h}_{\mathrm{B}}} \|\mathbf{w}\|_2 \geq t, && \text{(43b)} \\ & |\mathbf{h}^{\mathrm{T}}(\theta, \phi)\, \mathbf{w}| \leq \alpha t \quad \forall (\theta, \phi) \in \ddot{\Theta} \times \ddot{\Phi}, && \text{(43c)} \end{aligned}$$

where the components of $\mathbf{h}(\theta, \phi)$ are obtained with (6b), and $\ddot{\Theta}$ and $\ddot{\Phi}$ are fine grids on the intervals $[\theta_{\min}, \theta_{\max}]$ and $[\phi_{\min}, \phi_{\max}]$, respectively.

C. Uncertain LEDs Half-Angle

The emission pattern of the LEDs is fully determined by the Lambertian order

$$m = -1/\log_2(\cos \zeta^{\text{3-dB}}), \tag{44}$$

where $\zeta^{\text{3-dB}}$ is the half-intensity angle, or simply the half-angle, of the LEDs. This angle is typically specified by the LED manufacturer as a nominal value in the datasheet. In practice, however, the actual angle of each LED will deviate from the nominal value. In this subsection, we study channel uncertainty caused by this deviation. In particular, we assume an interval uncertainty model in which $\zeta^{\text{3-dB}} \in [\zeta_{\min}^{\text{3-dB}}, \zeta_{\max}^{\text{3-dB}}]$, and allow independent realizations of $\zeta^{\text{3-dB}}$ for each LED. Then, we map the interval $[\zeta_{\min}^{\text{3-dB}}, \zeta_{\max}^{\text{3-dB}}]$ into independent interval uncertainties for each entry of $\mathbf{h}_{\mathrm{E}}$.

We begin with rewriting the channel gain from (6a) as

$$h_i(m_i) = \kappa_i (m_i + 1)(\cos \zeta_i)^{m_i}, \quad i = 1, \ldots, N, \tag{45a}$$

where

$$m_i = -1/\log_2(\cos \zeta_i^{\text{3-dB}}), \quad \zeta_i^{\text{3-dB}} \in \left[\zeta_{\min}^{\text{3-dB}}, \zeta_{\max}^{\text{3-dB}}\right], \tag{45b}$$

and

$$\kappa_i \triangleq \frac{A}{2\pi \|\mathbf{d}_i\|_2^2} T_s\, g_{\mathrm{c}} \cos \psi_i\, I_{\Psi_{\mathrm{E}}}(\psi_i). \tag{45c}$$

Next, we define $m_{\min}$ and $m_{\max}$, respectively, as

$$m_{\min} \triangleq -1/\log_2(\cos \zeta_{\max}^{\text{3-dB}}), \tag{46a}$$

$$m_{\max} \triangleq -1/\log_2(\cos \zeta_{\min}^{\text{3-dB}}). \tag{46b}$$

Then, in order to map the interval $[m_{\min}, m_{\max}]$ into $[h_i^{\min}, h_i^{\max}]$, $i = 1, \ldots, N$, we first show that h_i is a quasiconcave function of m_i. Differentiating h_i with respect to m_i, we obtain

$$h_i'(m_i) = \kappa_i (\cos \zeta_i)^{m_i} (1 + (m_i + 1) \log_e(\cos \zeta_i)). \tag{47}$$

From (47), for $\kappa_i \neq 0$, $i = 1, \ldots, N$, we note that

$$\begin{cases} h_i'(m_i) \geq 0 & \text{for } m_i \leq m_i^\star, \\ h_i'(m_i) < 0 & \text{for } m_i > m_i^\star, \end{cases}$$

where $m_i^\star \triangleq -(1 + 1/\log_e(\cos \zeta_i))$, i.e., $h_i(m_i)$ is quasiconcave with global maximizer $m_i^\star$. Thus, the uncertainty set $\mathcal{H}_{\mathrm{E}}^{\zeta^{\text{3-dB}}}$ corresponding to the interval $[\zeta_{\min}^{\text{3-dB}}, \zeta_{\max}^{\text{3-dB}}]$ can be written as

$$\mathcal{H}_{\mathrm{E}}^{\zeta^{\text{3-dB}}} = \left\{ [h_1 \ \ldots \ h_N]^{\mathrm{T}} : h_i \in [h_i^{\min}, h_i^{\max}], i = 1, \ldots, N \right\}, \tag{48a}$$

where, for $i = 1, \ldots, N$,

$$h_i^{\min} = \begin{cases} h_i(m_{\min}) & \text{for } m_i^\star > m_{\max}, \\ \min\{h_i(m_{\min}), h_i(m_{\max})\} & \text{for } m_i^\star \in [m_{\min}, m_{\max}], \\ h_i(m_{\max}) & \text{for } m_i^\star < m_{\min}, \end{cases} \tag{48b}$$

$$h_i^{\max} = \begin{cases} h_i(m_{\max}) & \text{for } m_i^\star > m_{\max}, \\ h_i(m_i^\star) & \text{for } m_i^\star \in [m_{\min}, m_{\max}], \\ h_i(m_{\min}) & \text{for } m_i^\star < m_{\min}. \end{cases} \tag{48c}$$

Define $\hat{\mathbf{h}} \in \mathbb{R}_+^N$ and $\hat{\mathbf{H}} \in \mathbb{R}_+^{N \times N}$, respectively, as

$$\hat{\mathbf{h}} \triangleq \frac{1}{2}[h_1^{\max} + h_1^{\min} \ \ldots \ h_N^{\max} + h_N^{\min}]^{\mathrm{T}}, \tag{49a}$$

$$\hat{\mathbf{H}} \triangleq \frac{1}{2}\mathbf{Diag}(h_1^{\max} - h_1^{\min}, \ldots, h_N^{\max} - h_N^{\min}). \tag{49b}$$

Then, $\mathcal{H}_{\mathrm{E}}^{\zeta^{\text{3-dB}}}$ can be written as

$$\mathcal{H}_{\mathrm{E}}^{\zeta^{\text{3-dB}}} = \left\{ \hat{\mathbf{h}} + \hat{\mathbf{H}} \boldsymbol{v} : \boldsymbol{v} \in \mathbb{R}^N, \|\boldsymbol{v}\|_\infty \leq 1 \right\}. \tag{50}$$

Similar to (30)–(32), substituting with $\mathcal{H}_{\mathrm{E}}^{\boldsymbol{\zeta}^{\text{3-dB}}}$ into (19c), the problem in (19) can be expressed as

$$\begin{aligned} \underset{\|\mathbf{w}\|_\infty \le 1, t}{\text{maximize}} \quad & t && \text{(51a)} \\ \text{s.t.} \quad & \hat{\mathbf{h}}_{\mathrm{B}}^{\mathrm{T}}\mathbf{w} - \epsilon_{\mathbf{h}_{\mathrm{B}}}\|\mathbf{w}\|_2 \ge t, && \text{(51b)} \\ & \hat{\mathbf{h}}^{\mathrm{T}}\mathbf{w} + \|\hat{\mathbf{H}}\mathbf{w}\|_1 \le \alpha t, && \text{(51c)} \\ & \hat{\mathbf{h}}^{\mathrm{T}}\mathbf{w} - \|\hat{\mathbf{H}}\mathbf{w}\|_1 \ge -\alpha t. && \text{(51d)} \end{aligned}$$

D. Uncertain NLoS Components

In this subsection, we consider channel uncertainty arising from the NLoS components caused by diffuse reflections from nearby surfaces. Taking into account signal contributions from both the LoS and NLoS paths, the DC optical channel gain can be written as

$$h_i = h_i^{\text{LoS}} + h_i^{\text{NLoS}}, \quad i = 1, \ldots, N, \tag{52}$$

where h_i^{LoS} is the LoS component obtained with (6), and h_i^{NLoS} is the unknown NLoS component. We shall consider a simple multiplicative uncertainty model in which h_i^{NLoS} is an uncertain fraction, γ_i, of h_i^{LoS}, that is

$$h_i^{\text{NLoS}} = \gamma_i h_i^{\text{LoS}}, \quad 0 \le \gamma_i \le \gamma_{\max}, \, i = 1, \ldots, N, \tag{53}$$

where $\gamma_{\max} \triangleq \max\limits_i \gamma_i$. The actual value of $\gamma_{\max}$ depends mostly on the problem geometry as well as the diffuse reflectivity of nearby surfaces. In practice, $\gamma_{\max}$ can be measured or predicted using numerical simulations. Simulation results reported in [6] show $\gamma_{\max}$ of about 12% (see the discussion after Figure 6 in [6]). Note that the multiplicative model in (53) is applicable only when the LoS path between the ith LED and the photodetector exists, i.e., $h_i^{\text{LoS}} \neq 0$, and is dominant. In other words, (53) does not take into account the case in which the received signal consists entirely of NLoS components, e.g., when the LoS path is blocked or outside the receiver FoV.

From (52) and (53), the set of all possible channel gain vectors can be written as

$$\begin{aligned} &\mathcal{H}_{\mathrm{E}}^{\gamma_{\max}} = \\ &\left\{[h_1 \ \ldots \ h_N]^{\mathrm{T}} : h_i \in [h_i^{\text{LoS}}, (1+\gamma_{\max})h_i^{\text{LoS}}], i = 1, \ldots, N\right\}, \end{aligned} \tag{54}$$

which is similar to $\mathcal{H}_{\mathrm{E}}^{\boldsymbol{\zeta}^{\text{3-dB}}}$ in (48a), and thus we can proceed with the same steps from the previous subsection.

E. Combined Uncertainties

So far we have derived separate sets corresponding to uncertainties in location, orientation, half-angle, and NLoS components. In practice, however, these uncertainties may happen in combination with each other. Thus, more inclusive sets that take into account the aggregate uncertainty are required. Unfortunately, it is difficult, in general, to derive such sets or provide a unified treatment for different combinations of uncertainties because, as we mentioned earlier, the channel gain expression in (6) is a complex function of the uncertainty sources. Nevertheless, one intuitive approach to circumvent such a difficulty is to sample the channel gain vector over the variables with lower dimension or smaller uncertainty size. Consider, for example, the case of uncertain location and LEDs half-angle, that is

$$\begin{aligned} \mathcal{H}_{\mathrm{E}}^{\mathcal{B}\times\boldsymbol{\zeta}^{\text{3-dB}}} &= \mathcal{H}_{\mathrm{E}}^{\mathcal{B}} \times \mathcal{H}_{\mathrm{E}}^{\boldsymbol{\zeta}^{\text{3-dB}}} \\ &= \left\{\mathbf{h}(\boldsymbol{\delta}, \boldsymbol{\zeta}^{\text{3-dB}}) : \boldsymbol{\delta} \in \mathcal{B}, \, \boldsymbol{\zeta}^{\text{3-dB}} \in [\zeta_{\min}^{\text{3-dB}}, \zeta_{\max}^{\text{3-dB}}]^N\right\}, \end{aligned}$$

where $\boldsymbol{\zeta}^{\text{3-dB}} = [\zeta_1^{\text{3-dB}} \ \ldots \ \zeta_N^{\text{3-dB}}]^{\mathrm{T}}$. If $N > 3$, i.e., the dimension of $\boldsymbol{\zeta}^{\text{3-dB}}$ is bigger than the dimension of $\boldsymbol{\delta}$, then $\mathcal{B}$ can be discretized using a three-dimensional K-point grid, $\ddot{\mathcal{B}} = \{\boldsymbol{\delta}_1, \ldots, \boldsymbol{\delta}_K\}$, and the problem in (51) is modified to

$$\begin{aligned} \underset{\|\mathbf{w}\|_\infty \le 1, t}{\text{maximize}} \quad & t \\ \text{s.t.} \quad & \hat{\mathbf{h}}_{\mathrm{B}}^{\mathrm{T}}\mathbf{w} - \epsilon_{\mathbf{h}_{\mathrm{B}}}\|\mathbf{w}\|_2 \ge t, \\ & \hat{\mathbf{h}}_k^{\mathrm{T}}\mathbf{w} + \|\hat{\mathbf{H}}_k\mathbf{w}\|_1 \le \alpha t, \\ & \hat{\mathbf{h}}_k^{\mathrm{T}}\mathbf{w} - \|\hat{\mathbf{H}}_k\mathbf{w}\|_1 \ge -\alpha t, \qquad k = 1, \ldots, K, \end{aligned}$$

where $\hat{\mathbf{h}}_k$ and $\hat{\mathbf{H}}_k$ are obtained as in (49) using the components of $\mathbf{h}^{\min}(\boldsymbol{\delta}_k)$ and $\mathbf{h}^{\max}(\boldsymbol{\delta}_k)$, for $k = 1, \ldots, K$. The same idea can be applied to other combinations of uncertainty sources.

Furthermore, there exist specific cases of combined uncertainties in which discretization may not be necessary. Consider, for example, the special, but practically relevant, case of small location and angle uncertainties. With such a combination, the linear channel gain models considered in Sections IV-A1 and IV-B1 are both applicable, and an explicit formulation of the optimization problem can be obtained as follows. First, we rewrite the linearized channel gain expression from (28) as

$$\begin{aligned} \bar{\mathbf{h}}(\boldsymbol{\delta}, \mathbf{u}) &= \mathbf{h_0} + \mathbf{J_0}\boldsymbol{\delta} \\ &= \mathbf{D}\mathbf{u} + \mathbf{G_0}(\mathbf{I}_3 \otimes \mathbf{u})\boldsymbol{\delta} \\ &= \mathbf{D}\mathbf{u} + \mathbf{G_0}(\boldsymbol{\delta} \otimes \mathbf{I}_3)\mathbf{u}, \end{aligned} \tag{55}$$

where $\mathbf{D}$ is as defined in (37), and the entires of $\mathbf{G_0}$, $\mathbf{G_0} \in \mathbb{R}^{N\times 9}$, can be inferred from (90b)–(90d) in Appendix D. Then, the inner problem (19) can be expressed as

$$\begin{aligned} \underset{\|\mathbf{w}\|_\infty \le 1, t}{\text{maximize}} \quad & t && \text{(56a)} \\ \text{s.t.} \quad & \hat{\mathbf{h}}_{\mathrm{B}}^{\mathrm{T}}\mathbf{w} - \epsilon_{\mathbf{h}_{\mathrm{B}}}\|\mathbf{w}\|_2 \ge t, && \text{(56b)} \\ & \max_{\substack{\boldsymbol{\delta}\in\mathcal{B} \\ \|\mathbf{u}\|_2 \le 1}} |\mathbf{u}^{\mathrm{T}}\mathbf{D}^{\mathrm{T}}\mathbf{w} + \mathbf{u}^{\mathrm{T}}(\boldsymbol{\delta}^{\mathrm{T}} \otimes \mathbf{I}_3)\mathbf{G_0}^{\mathrm{T}}\mathbf{w}| \le \alpha t. && \text{(56c)} \end{aligned}$$

The constraint in (56c) can be replaced by a set of second-order cone constraints, given by

$$\|\mathbf{D}^{\mathrm{T}}\mathbf{w} + (\mathbf{v}_{(k)}^{\mathrm{T}} \otimes \mathbf{I}_3)\mathbf{G_0}^{\mathrm{T}}\mathbf{w}\|_2 \le \alpha t, \quad k = 1, \ldots, 8, \tag{57}$$

where $\mathbf{v}_{(k)} \in \mathbb{R}^3$, $k = 1, \ldots, 8$, are the vertices (or corners) of $\mathcal{B}$.

V. Numerical Examples

In this section, we provide numerical examples to verify the performance gains of the beamformers proposed in Section III compared to conventional beamforming schemes. We also demonstrate the design of robust beamformers in a typical VLC scenario and investigate the resulting worst-case secrecy rate performance under different uncertainty levels.

A. Performance Comparisons

All the results presented in this subsection are obtained under the following assumptions. The number of transmit elements is set to $N = 4$. The entries of $\mathbf{h}_{\mathrm{B}}$ and $\mathbf{h}_{\mathrm{E}}$ are generated i.i.d. according to the uniform distribution over the interval $[0, 1]$, and the results are averaged over 1000 independent trials. The optimal and robust beamformers are obtained via Algorithm 1, where the outer maximization problem is solved with accuracy $\epsilon_\alpha = 0.2$ dB and the inner problem is solved using the CVX toolbox [27] along with the MOSEK solver [29].

1) Optimal versus suboptimal beamformers under different l_p-norm constraints: In this example, we compare the secrecy rate performance of the optimal beamformer with the generalized eigenvector (GEV) and ZF beamformers, under the premise of perfect channel information.

Figure 3(a) depicts the secrecy rates (8) versus P/σ. The secrecy rates are obtained with $\mathbf{w}_{\alpha^\star}$, $\mathbf{w}_{\mathrm{GEV}}$, and $\mathbf{w}_{\alpha=0}$, corresponding to the optimal, GEV, and ZF beamformers, respectively, subject to the constraint $\|\mathbf{w}\|_p \leq 1$, for $p = 1, 2, \infty$. The optimal beamformer $\mathbf{w}_{\alpha^\star}$ is obtained with Proposition 1, and the corresponding $\alpha^\star$ is shown in Figure 3(b). The beamformer $\mathbf{w}_{\mathrm{GEV}}$ is the generalized eigenvector of the matrix pair $(6P^2\mathbf{h}_{\mathrm{B}}\mathbf{h}_{\mathrm{B}}^{\mathrm{T}}+3\pi e\sigma^2\mathbf{I}_N, \pi eP^2\mathbf{h}_{\mathrm{E}}\mathbf{h}_{\mathrm{E}}^{\mathrm{T}}+3\pi e\sigma^2\mathbf{I}_N)$ corresponding to its largest generalized eigenvalue, where $\mathbf{w}_{\mathrm{GEV}}$ is scaled such that $\|\mathbf{w}_{\mathrm{GEV}}\|_p = 1$, for $p = 1, 2, \infty$. The ZF beamformer $\mathbf{w}_{\alpha=0}$ is obtained by solving (14) with $\alpha = 0$.

As expected, we note from Figure 3(a) that the optimal beamformer provides the best performance for all $p = 1, 2, \infty$, however at the cost of increased complexity. We also note that the secrecy rates of the optimal and GEV beamformers coincide when $p = 2$. This is because GEV beamforming is optimal under the l_2-norm constraint [10]. Furthermore, we note that the ZF beamformer outperforms its GEV counterpart under the l_∞-norm constraint, and it approaches the performance of the optimal beamformer as P/σ increases. Figure 3(b) shows that $\alpha^\star$ is nonincreasing with respect to P/σ for all $p = 1, 2, \infty$. Thus, the ZF beamformer is in fact asymptotically optimal at high P/σ for all p. Moreover, it can be observed that $\alpha^\star$ decreases rapidly as p increases. This reveals that the performance gap between the ZF and optimal beamformers narrows quickly with increasing p at high P/σ.

Figure 4 shows the secrecy rate performance versus the number of eavesdroppers K when $20\log_{10}(P/\sigma) = 20$ dB. Each eavesdropper has a single receive element, and there is no collaboration among the eavesdroppers, i.e., centralized processing of the received signals is not permitted. The secrecy rates are obtained with

$$R_{\mathrm{s}}(\mathbf{w}) = \left[\frac{1}{2}\log_2 \frac{6P^2(\mathbf{h}_{\mathrm{B}}^{\mathrm{T}}\mathbf{w})^2 + 3\pi e\sigma^2}{\pi eP^2\|\mathbf{H}_{\mathrm{E}}^{\mathrm{T}}\mathbf{w}\|_\infty^2 + 3\pi e\sigma^2}\right]^+, \qquad (58)$$

where $\mathbf{H}_{\mathrm{E}} \triangleq [\mathbf{h}_{\mathrm{E}_1} \ \ldots \ \mathbf{h}_{\mathrm{E}_K}]$. The GEV beamformer is the generalized eigenvector of the matrix pair $(6P^2\mathbf{h}_{\mathrm{B}}\mathbf{h}_{\mathrm{B}}^{\mathrm{T}} + 3\pi e\sigma^2\mathbf{I}_N, \pi eP^2\mathbf{H}_{\mathrm{E}}\mathbf{H}_{\mathrm{E}}^{\mathrm{T}} + 3\pi e\sigma^2\mathbf{I}_N)$ corresponding to the largest generalized eigenvalue. The optimal beamformer is obtained with Proposition 1 after replacing the constraint in (14b) with $\|\mathbf{H}_{\mathrm{E}}^{\mathrm{T}}\mathbf{w}\|_\infty \leq \alpha\mathbf{h}_{\mathrm{B}}^{\mathrm{T}}\mathbf{w}$, and the ZF beamformer is obtained by setting $\alpha = 0$.

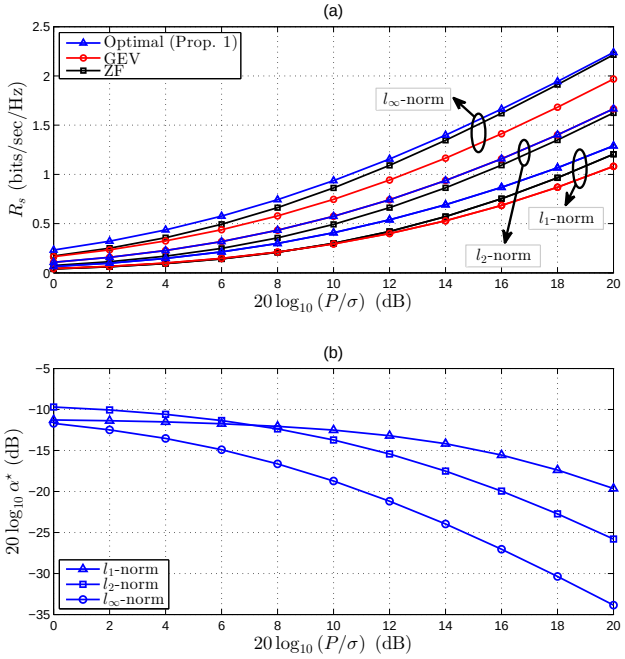

Fig. 3. (a) Secrecy rates (8) obtained with the optimal, GEV, and ZF beamformers versus P/σ, subject to the constraint $\|\mathbf{w}\|_p \leq 1$, for $p = 1, 2, \infty$. (b) $\alpha^\star$ corresponding to the optimal beamformer $\mathbf{w}_{\alpha^\star}$.

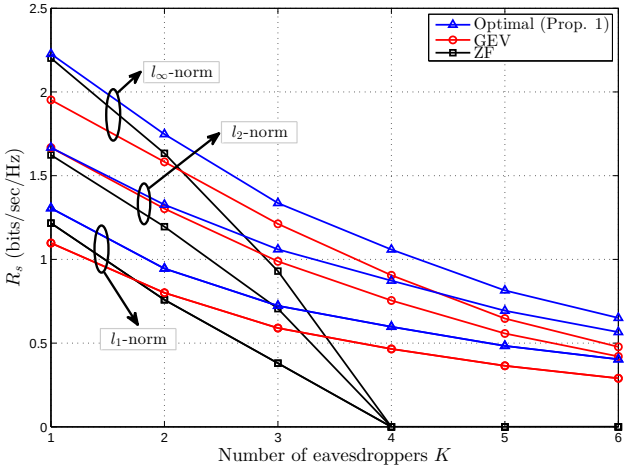

Fig. 4. Secrecy rates (58) of the optimal, GEV, and ZF beamformers under different l_p-norm constraints, versus the number of eavesdroppers when $20\log_{10}(P/\sigma) = 20$ dB.

We note that the GEV beamformer is optimal when $K = 1$ and $p = 2$. We also note that, as K increases, the GEV beamformer outperforms the ZF scheme even when $p \neq 2$. Obviously, ZF becomes infeasible once $K \geq N$.

2) Robust versus non-robust schemes: In this example, we compare the worst-case secrecy rate performance of the robust beamformer with non-robust schemes. We assume that the uncertainty sets for Bob's and Eve's channels, respectively, are given by

$$\mathcal{H}_{\mathrm{B}} = \left\{\hat{\mathbf{h}}_{\mathrm{B}} + \mathbf{e}_{\mathbf{h}_{\mathrm{B}}} : \|\mathbf{e}_{\mathbf{h}_{\mathrm{B}}}\|_2 \leq \epsilon_{\mathbf{h}_{\mathrm{B}}}\right\}, \qquad (59a)$$

$$\mathcal{H}_{\mathrm{E}} = \left\{\hat{\mathbf{h}}_{\mathrm{E}} + \mathbf{e}_{\mathbf{h}_{\mathrm{E}}} : \|\mathbf{e}_{\mathbf{h}_{\mathrm{E}}}\|_\infty \leq \epsilon_{\mathbf{h}_{\mathrm{E}}}\right\}. \qquad (59b)$$

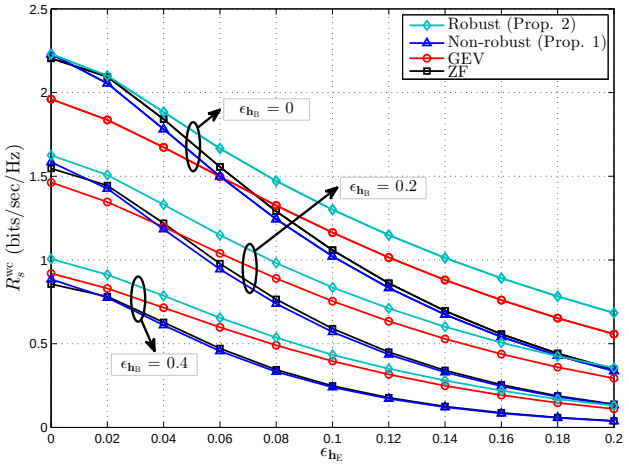

Fig. 5. Worst-case secrecy rates (60) of the robust, non-robust, GEV, and ZF beamformers versus $\epsilon_{\mathbf{h}_\mathrm{E}}$ with $\epsilon_{\mathbf{h}_\mathrm{B}} = 0, 0.2, 0.4$. All beamformers are subject to the amplitude constraint $\|\mathbf{w}\|_\infty \leq 1$, and $20\log_{10}(P/\sigma) = 20$ dB.

The entries of the nominal vectors $\hat{\mathbf{h}}_\mathrm{B}$ and $\hat{\mathbf{h}}_\mathrm{E}$ are generated at random, and the results are averaged over 1000 trials.

In Figure 5, we plot the worst-case secrecy rate

$$R_\mathrm{s}^\mathrm{wc}(\mathbf{w}) = \left[\frac{1}{2}\log_2 \frac{\min\limits_{\mathbf{h}_\mathrm{B}\in\mathcal{H}_\mathrm{B}} 6P^2(\mathbf{h}_\mathrm{B}^\mathrm{T}\mathbf{w})^2 + 3\pi e\sigma^2}{\max\limits_{\mathbf{h}_\mathrm{E}\in\mathcal{H}_\mathrm{E}} \pi e P^2(\mathbf{h}_\mathrm{E}^\mathrm{T}\mathbf{w})^2 + 3\pi e\sigma^2}\right]^+ \tag{60}$$

versus $\epsilon_{\mathbf{h}_\mathrm{E}}$, for $\epsilon_{\mathbf{h}_\mathrm{B}} = 0, 0.2, 0.4$, and $20\log_{10}(P/\sigma) = 20$ dB. We compare the performance of the robust beamformer from Proposition 2 with its non-robust counterpart from Proposition 1, as well as the GEV and ZF beamformers. All beamformers are subject to the amplitude constraint $\|\mathbf{w}\|_\infty \leq 1$. Substituting from (59a) and (59b) into (19b) and (19c), respectively, the inner problem (19) is expressed as

$$\underset{\|\mathbf{w}\|_\infty \leq 1, t}{\text{maximize}} \quad t \tag{61a}$$

$$\text{s.t.} \quad \hat{\mathbf{h}}_\mathrm{B}^\mathrm{T}\mathbf{w} - \epsilon_{\mathbf{h}_\mathrm{B}}\|\mathbf{w}\|_2 \geq t, \tag{61b}$$

$$\hat{\mathbf{h}}_\mathrm{E}^\mathrm{T}\mathbf{w} + \epsilon_{\mathbf{h}_\mathrm{E}}\|\mathbf{w}\|_1 \leq \alpha t, \tag{61c}$$

$$\hat{\mathbf{h}}_\mathrm{E}^\mathrm{T}\mathbf{w} - \epsilon_{\mathbf{h}_\mathrm{E}}\|\mathbf{w}\|_1 \geq -\alpha t. \tag{61d}$$

Then, the robust beamformer is obtained via Algorithm 1. On the other hand, the non-robust, GEV, and ZF beamformers are obtained using the nominal vectors $\hat{\mathbf{h}}_\mathrm{B}$ and $\hat{\mathbf{h}}_\mathrm{E}$.

As expected, we note from Figure 5 that the robust beamformer outperforms its non-robust counterparts, clearly at the expense of increased computational complexity, and the performance gain becomes more evident with increasing $\epsilon_{\mathbf{h}_\mathrm{B}}$ and $\epsilon_{\mathbf{h}_\mathrm{E}}$.

B. Worst-Case Secrecy Rate Performance in VLC Scenarios

In this subsection, we investigate the worst-case secrecy rate performance in a typical VLC scenario using the robust beamformer from Proposition 2 along with the uncertainty sets derived in Section IV.

We consider a room of size $5 \times 5 \times 3$ m^3 illuminated by 25 square-shaped lighting fixtures uniformly distributed over 4×4 m^2 of the ceiling area, as depicted in Figure 6. Each

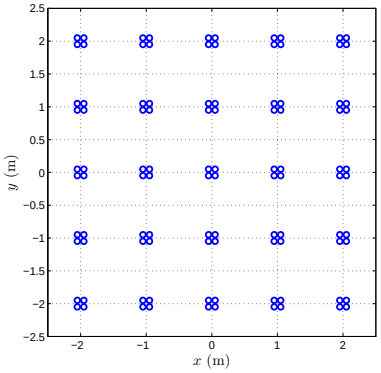

Fig. 6. Layout of the LEDs on the ceiling. There exist 25 lighting fixtures. Each fixture is 10×10 cm^2 and encloses four LEDs located at the corners of the fixture.

TABLE I
SIMULATION PARAMETERS.

Simulation setup	
Room size	$5 \times 5 \times 3$ m^3
Number of fixtures N_Fix	25
Fixture size	10×10 cm^2
Number of LEDs per fixture N_LED	4
Total number of LEDs N	100
LED electrical and optical characteristics	
Forward voltage	3.6 V
Forward current I_DC	700 mA
Input electrical power	2.52 W
Optical power / current η	813.6 μW/mA
Output optical power (or radiant flux) P_opt	569.52 mW
Luminous efficiency (warm-white color)	284 lm/W
Luminous flux	161.74 lm
Luminous efficacy	64.18 lm/W
Nominal half-intensity angle $\zeta^{\text{3-dB}}$	60°
Peak (center) luminous intensity	51.48 cd
Modulation index μ	10%
Optical receiver characteristics	
Gain of the optical filter T_s	1
Lens refractive index n_r	1.5
Photodetector responsivity R	100 μA/mW/cm^2
Photodetector area A	1 cm^2

fixture occupies 10×10 cm^2 and encloses four high-brightness 2.5-W LEDs located at the corners of the fixture. Each LED radiates 570 mW optical power (or radiant flux). Emitted light is "warm-white" (i.e., color temperature is between 2700 and 3000 K) with luminous efficiency 284 lm/W [30, Table 3.2]. The resulting luminous flux is $0.570 \times 284 \approx 162$ lm per LED. The nominal half-intensity angle (measured from the center) is 60°, and the peak (or center) luminous intensity is 51 cd. The resulting illuminance, averaged over a horizontal 4×4 m^2 illumination grid at height 0.85 m above the floor level, is 339 Lux. For convenience, all simulation parameters are provided in Table I.

All the following results are generated with Bob and Eve having photodetectors of area $A = 1$ cm^2 and responsivity $R = 100$ μA/mW/cm^2. The modulation index μ is set at 10%. The noise power is assumed to be equal everywhere with $20\log_{10}\sigma = -114$ dBm. This value is obtained with [31, Eq. (6)] using the average received DC optical power (averaged over the horizontal plane at height 0.85 m) with FoV $\Psi = 70°$ and receiver bandwidth of 10 MHz. All location coordinates are specified in meters with respect to the room center at the floor level.

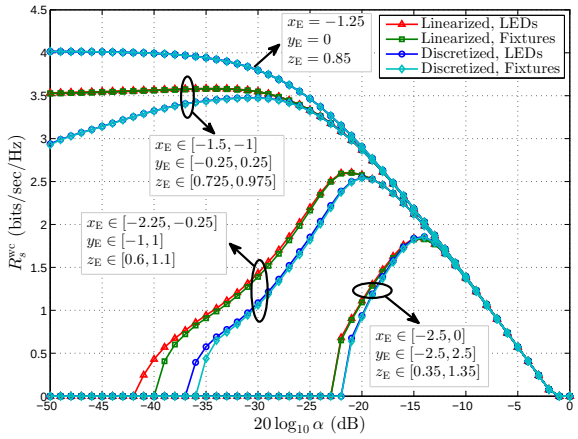

Fig. 7. Worst-case secrecy rate (20) versus α with uncertain Eve's location. $\theta_E = 0$ and $\Psi_E = 70°$.

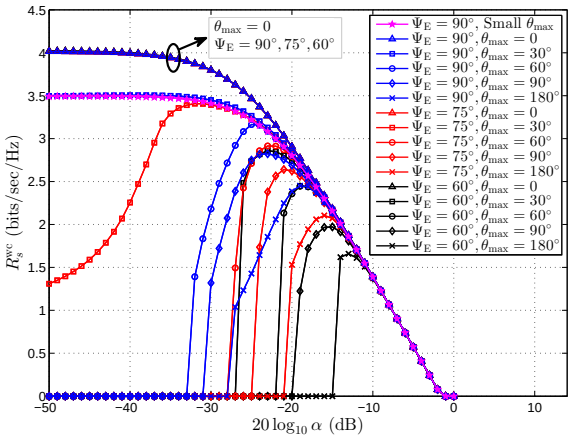

Fig. 8. Worst-case secrecy rate (20) versus α with uncertain Eve's orientation. $x_E = -1.25$, $y_E = 0$, $z_E = 0.85$, $\theta_E \in [0, \theta_{max}]$, and $\phi_E \in [0, 360°]$.

In all scenarios, we assume that Bob is located at $(x_B, y_B, z_B) = (1.7173, 0.7496, 0.85)$ with orientation $(\theta_B, \phi_B) = (15°, 240°)$ and FoV $\Psi_B = 70°$. Furthermore, we use the spherical set in (21) to model uncertainty in Bob's channel, where the entries of $\hat{\mathbf{h}}_B$ are obtained with (6), i.e., $\hat{\mathbf{h}}_B = \mathbf{h}(x_B, y_B, z_B, \theta_B, \phi_B, \Psi_B)$, and $\epsilon_{\mathbf{h}_B} = 0.1\|\hat{\mathbf{h}}_B\|_2$. The nominal estimate $\hat{\mathbf{h}}_B$ is fixed and assumed to be known to Alice via feedback from Bob. Parameters relevant to Eve are provided in the caption of each figure. In all cases, for the sake of illustration, we plot the worst-case secrecy rate versus α using (20), where $20 \log_{10} \alpha = -50, -49, \ldots, 0$ dB. We also include the case of certain Eve's channel for comparison purposes. For each α, we use the CVX toolbox [27], in conjunction with the MOSEK solver [29], to solve (19) using the relevant uncertainty set $\mathcal{H}_E$ from Section IV.

1) Uncertain eavesdropper's location: Figure 7 shows the worst-case secrecy rate performance with uncertain Eve's location. We include three groups of curves corresponding to three uncertainty regions, $\mathcal{B}$, of different volumes. All the regions are rectangular and centered at $(x, y, z) = (-1.25, 0, 0.85)$. Four curves are generated for each $\mathcal{B}$ corresponding to the combinations of two methods to approximate $\mathcal{H}_E^{\mathcal{B}}$ and two methods to modulate the LEDs. We refer to the case in which the affine approximation (28) is used as "Linearized", and to the case in which $\mathcal{B}$ is discretized as "Discretized". For the "Linearized" case, $\mathcal{B}$ is divided into identical boxes, each of volume $2l_x \times 2l_y \times 2l_z = 0.5 \times 0.5 \times 0.25$ m^3, then (28) is applied to each box and $\mathbf{w}_\alpha$ is obtained with (32). For the "Discretized" case, $\mathcal{H}_E^{\mathcal{B}}$ is approximated by sampling the channel gain in the three-dimensional space using a $10 \times 10 \times 10$ cm^3 grid, and $\mathbf{w}_\alpha$ is obtained with (34). Furthermore, we refer to the case in which each LED is modulated independently as "LEDs", and to the case in which all LEDs in one fixture are modulated with the same current signal as "Fixtures".

As expected, we note from Figure 7 that R_s^{wc} decreases as the uncertainty about Eve's location increases. For the case of certain Eve's location, we can see that the ZF beamformer is practically optimal. In addition, Figure 7 reveals that independent-LED modulation does not provide much improvement, if any, compared to the more practical and less expensive "Fixture" modulation scheme. This result is also expected since LEDs in the same fixture are relatively close to each other and have almost identical channel gains. Figure 7 also verifies the validity of the affine approximation in (28) when l_x, l_y, and l_z are chosen properly.

2) Uncertain eavesdropper's orientation: In Figure 8, we plot the worst-case secrecy rate performance with uncertain Eve's orientation. We also investigate the impact of Eve's FoV on the secrecy rate. The curve "Small θ_{max}" is generated with $\mathbf{w}_\alpha$ obtained from (42), whereas all other curves are obtained with (43) after discretizing the intervals $\Theta = [0, \theta_{max}]$ and $\Phi = [0, 360°]$ using $\Delta_\theta = \Delta_\phi = 4°$.

For the case $\theta_{max} = 0$, i.e., no uncertainty about Eve's orientation, we can see that ZF is essentially optimal. We also note that the curve "Small θ_{max}" almost coincides with the curve corresponding to $\Psi_E = 90°$ and $\theta_{max} = 30°$. Thus, the linear channel gain model that leads to the problem in (42) is indeed valid for small angle variations and wide FoV. Figure 8 also reveals that reducing Eve's FoV has a negative impact on the secrecy rate performance, which can be explained as follows. First, we see from (7) that reducing the FoV of the concentrator increases its gain inside the FoV. Second, the limited FoV of Eve's receiver, in conjunction with her ability to adjust orientation, increases her received signal space as measured by the number of nonzero singular values of the matrix $\mathbf{H}_E^{\ddot{\mathcal{U}}}$ whose columns are the elements of the discretized uncertainty set $\mathcal{H}_E^{\ddot{\mathcal{U}}}$. Obviously, increasing the signal space available to Eve makes it more difficult for Alice to suppress Eve's signal, i.e., more of the degrees of freedom available to Alice are exploited, and thus the secrecy rate is reduced.

3) Uncertain eavesdropper's location and LEDs half-angle: Figure 9 depicts the secrecy performance with uncertain Eve's location and LEDs half-angle. We consider half-angle uncertainties up to $\pm 20°$ around the nominal value of $60°$, and the location uncertainty region $\{(x_E, y_E) : x_E \in [-2.25, -0.25], y_E \in [-2.5, 2.5]\}$ is discretized using $\Delta_x = \Delta_y = 20$ cm. As can be seen,

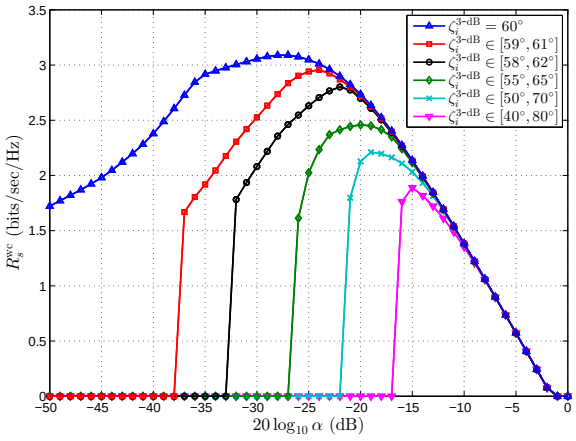

Fig. 9. Worst-case secrecy rate (20) versus α with uncertain Eve's location and LEDs half-angle $\zeta_i^{3\text{-dB}}$, $i = 1, \ldots, N$. $x_{\text{E}} \in [-2.25, -0.25]$, $y_{\text{E}} \in [-2.5, 2.5]$, $z_{\text{E}} = 0.85$, $\theta_{\text{E}} = 0$, and $\Psi_{\text{E}} = 70°$.

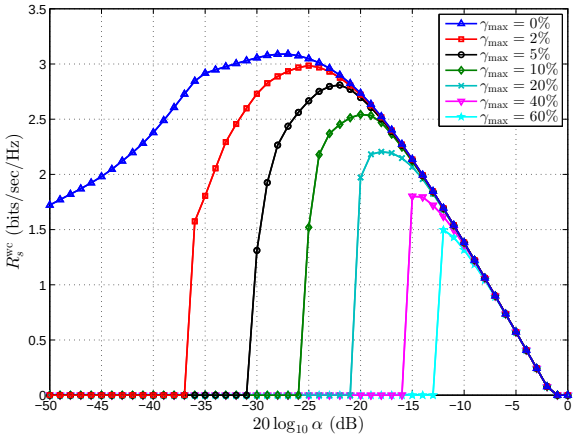

Fig. 10. Worst-case secrecy rate (20) versus α with uncertain Eve's location and NLoS components. $x_{\text{E}} \in [-2.25, -0.25]$, $y_{\text{E}} \in [-2.5, 2.5]$, $z_{\text{E}} = 0.85$, $\theta_{\text{E}} = 0$, and $\Psi_{\text{E}} = 70°$.

even relatively small half-angle deviations, e.g., $\pm 5°$, can significantly reduce the worst-case secrecy rate.

4) Uncertain eavesdropper's location and NLoS components: In Figure 10, we show the worst-case secrecy rate performance with uncertain location and NLoS components. Similar to the results in Figure 9, the location uncertainty region is discretized using $\Delta_x = \Delta_y = 20$ cm. We investigate the performance when the strength of the NLoS components can go up to $\gamma_{\max} = 60\%$ of the LoS path. Note that $\gamma_{\max} = 60\%$, or even 40%, is a too pessimistic or too conservative assumption. In typical scenarios with only diffuse reflections, i.e., no large windows or mirrors, $\gamma_{\max}$ will probably be less than 20% (see, e.g., Figure 4 in [32] or the discussion after Figure 6 in [6]).

VI. Conclusions

In this paper, we studied the design of transmit beamformers for secrecy rate maximization in MISO wiretap channels subject to amplitude constraints. Such constraints are typically difficult to handle and, because of that, they are often overlooked in favor of the more convenient total power constrains. We considered VLC systems as a prominent example in which amplitude constraints naturally arise because of limitations on the emitting devices. In fact, however, all digital transmitters experience some sort of amplitude constraints because of the digital-to-analog converters (DACs) incorporated to generate the analog signal that is ultimately released on the physical channel. Clearly, these DACs are limited in their dynamic range, and thus are better modelled with amplitude constraints. Therefore, apart from being an interesting and mathematically-challenging problem, we believe that taking amplitude constraints into account has practical significance, not only for intensity-modulation systems, but in fact for all digital transmitters.

We tackled the nonconvex secrecy rate maximization problem by transforming it into an equivalent quasiconvex line search problem. Our approach is conceptually simple but provably optimal for general l_p-norm constraints, and the equivalent problem itself is practically meaningful. Furthermore, our approach proved helpful in tackling the more complex robust design problem with uncertain channel information.

We also used the VLC scenario as a practical example in which reasonable estimates of the eavesdropper's channel can be obtained without feedback from the (passive) eavesdropper. Numerical results show that the excess degrees of freedom provided by the large number of LEDs in typical VLC scenarios can be effectively utilized to compensate for the lack of accurate information regarding the eavesdropper's channel.

Finally, it is worthwhile to mention that our approach in Propositions 1 and 2 takes advantage of the fact that the signal term in the numerator of the secrecy rate expression (8) is a *squared linear function* of the beamformer[4]. This ultimately leads to convex inner optimization problems, i.e., the problems in (14) and (19). If the legitimate receiver, however, has multiple receiving elements, such problems will no longer be convex, and the secrecy rate maximization problem is expected to be more difficult to solve. Thus, a natural extension to this work would be to consider linear precoding for the MIMO wiretap channel, subject to amplitude constrains.

Appendix A
Proof of Proposition 1

Our goal here is to prove that the problem in (11) is equivalent to the line search problem in (12), and the objective function in (12) is quasiconcave with respect to the search parameter α. The latter part, in particular, is not straightforward.

Using the auxiliary variable $\tau \geq 3\pi e \sigma^2$, the problem in (11) can be expressed as

$$\underset{\|\mathbf{w}\|_p \leq 1, \tau}{\text{maximize}} \quad \frac{6P^2(\mathbf{h}_{\text{B}}^{\text{T}}\mathbf{w})^2 + 3\pi e\sigma^2}{\tau} \tag{62a}$$

$$\text{s.t.} \quad \pi e P^2(\mathbf{h}_{\text{E}}^{\text{T}}\mathbf{w})^2 + 3\pi e\sigma^2 \leq \tau, \tag{62b}$$

or, equivalently,

$$\underset{\tau}{\text{maximize}} \ \frac{f(\tau)}{\tau}, \tag{63}$$

[4]The corresponding term in the denominator is also a squared linear function of the beamformer, but this is not critical because extension to the case in which only Eve has multiple receiving elements is not difficult.

where $f(\tau)$ is defined as

$$f(\tau) \triangleq \max_{\|\mathbf{w}\|_p \leq 1} \quad 6P^2(\mathbf{h}_\mathrm{B}^\mathrm{T}\mathbf{w})^2 + 3\pi e\sigma^2 \tag{64a}$$

$$\text{s.t.} \quad |\mathbf{h}_\mathrm{E}^\mathrm{T}\mathbf{w}| \leq \sqrt{\frac{\tau - 3\pi e\sigma^2}{\pi e P^2}}. \tag{64b}$$

Note that the constraints in (62b) and (64b) are equivalent. In the following, we show that the objective function in (63) is quasiconcave with respect to τ by establishing concavity of $f(\tau)$. First, we introduce a new variable $\varepsilon \geq 0$, defined as

$$\varepsilon \triangleq \sqrt{\frac{\tau - 3\pi e\sigma^2}{\pi e P^2}}. \tag{65}$$

We also define the *perturbation function* $\varphi(\varepsilon)$ as

$$\varphi(\varepsilon) \triangleq \max_{\|\mathbf{w}\|_p \leq 1} \quad \mathbf{h}_\mathrm{B}^\mathrm{T}\mathbf{w} \tag{66a}$$

$$\text{s.t.} \quad |\mathbf{h}_\mathrm{E}^\mathrm{T}\mathbf{w}| \leq \varepsilon. \tag{66b}$$

It is clear that $\varphi(\varepsilon)$ is nonnegative and nondecreasing for all $\varepsilon \geq 0$. Furthermore, the perturbed problem in (66) is convex, and thus $\varphi(\varepsilon)$ is concave [24, Section 5.6.1]. As a consequence, $\varphi(\varepsilon)$ is continuous and its *right and left derivatives*[5], $\varphi'_+(\varepsilon)$ and $\varphi'_-(\varepsilon)$, exist for all $\varepsilon > 0$. These derivatives are nonincreasing in the sense that, for any $\varepsilon_2 > \varepsilon_1 > 0$, we have [33, Theorem 1.6]

$$\varphi'_-(\varepsilon_1) \geq \varphi'_+(\varepsilon_1) \geq \varphi'_-(\varepsilon_2) \geq \varphi'_+(\varepsilon_2) \geq 0, \tag{67}$$

where the last inequality holds since $\varphi(\varepsilon)$ is nondecreasing. Moreover, for any $\varepsilon_0 \geq 0$ and any $\varepsilon \in \{\varepsilon : \varepsilon > 0, \varphi'_+(\varepsilon) = \varphi'_-(\varepsilon)\}$, i.e., any ε at which $\varphi(\varepsilon)$ is differentiable, we have [24, Section 3.1.3]

$$\varphi(\varepsilon_0) \leq \varphi(\varepsilon) + \varphi'(\varepsilon)(\varepsilon_0 - \varepsilon). \tag{68}$$

Substituting with $\varepsilon_0 = 0$ back into (68), we obtain

$$\varphi(\varepsilon) \geq \varphi(0) + \varepsilon\varphi'(\varepsilon) \geq \varepsilon\varphi'(\varepsilon), \tag{69}$$

where the last inequality follows from nonnegativity of $\varphi(0)$. We are now ready to prove that $f(\tau) = 6P^2(\varphi(\varepsilon))^2 + 3\pi e\sigma^2$ is concave with respect to $\tau = \pi e P^2\varepsilon^2 + 3\pi e\sigma^2$. The right and left derivatives of $f(\tau)$ can be written in terms of $\varphi'_+(\varepsilon)$ and $\varphi'_-(\varepsilon)$, respectively, as

$$f'_+(\tau) = \frac{6}{\pi e}\frac{\varphi(\varepsilon)}{\varepsilon}\varphi'_+(\varepsilon), \quad f'_-(\tau) = \frac{6}{\pi e}\frac{\varphi(\varepsilon)}{\varepsilon}\varphi'_-(\varepsilon). \tag{70}$$

From (67) and (70), it is clear that

$$f'_-(\tau) \geq f'_+(\tau) \quad \text{for any } \tau > 3\pi e\sigma^2. \tag{71}$$

Furthermore, when $\varphi(\varepsilon)$ is differentiable (and consequently $f(\tau)$ is differentiable), we have

$$\frac{\partial f'(\tau)}{\partial \tau} = \frac{3}{\pi e\varepsilon^2}\left(\left(\varphi'(\varepsilon) - \frac{\varphi(\varepsilon)}{\varepsilon}\right)\varphi'(\varepsilon) + \varphi(\varepsilon)\frac{\partial\varphi'(\varepsilon)}{\partial\varepsilon}\right) \leq 0, \tag{72}$$

[5]We resort to one-sided derivatives, rather than the ordinary two-sided derivative $\varphi'(\varepsilon)$, because $\varphi(\varepsilon)$ is not necessarily smooth or differentiable over the whole interior of its domain. Particularly, there exist, in general, some $\varepsilon > 0$ at which $\varphi'_+(\varepsilon) \neq \varphi'_-(\varepsilon)$. These are the points where $\varphi'_+(\varepsilon)$ and $\varphi'_-(\varepsilon)$ have jump discontinuities. Nevertheless, since $\varphi(\varepsilon)$ is concave, there are only countably many such jumps, i.e., the set $\{\varepsilon : \varepsilon > 0, \varphi'_+(\varepsilon) \neq \varphi'_-(\varepsilon)\}$ has zero Lebesgue measure [33, Section 1.8].

where the inequality holds since $\varphi'(\varepsilon) \leq \varphi(\varepsilon)/\varepsilon$, $\varphi'(\varepsilon) \geq 0$, $\varphi(\varepsilon) \geq 0$, and $\partial\varphi'(\varepsilon)/\partial\varepsilon \leq 0$ (the latter follows from (67) or the second-order condition of concavity [24, Section 3.1.4]). Combining (71) and (72) yields

$$f'_-(\tau_1) \geq f'_+(\tau_1) \geq f'_-(\tau_2) \geq f'_+(\tau_2), \tag{73}$$

for any $\tau_2 > \tau_1 > 3\pi e\sigma^2$. Hence, $f(\tau)$ is concave [34, Theorem 24.2]. Then, it is straightforward to establish that $f(\tau)/\tau$ is quasiconcave by noting that all the β-superlevel sets $\{\tau : \tau \geq 3\pi e\sigma^2,\ f(\tau)/\tau \geq \beta\}$, for all $\beta \in \mathbb{R}$, are convex, i.e., intervals, including, possibly, empty and unbounded intervals [24, Section 3.4.1].

Next, we define the new variable $\alpha \geq 0$ as

$$\alpha \triangleq \frac{\varepsilon}{\varphi(\varepsilon)} = \sqrt{\frac{\tau - 3\pi e\sigma^2}{\pi e P^2(\varphi(\varepsilon))^2}},\ \varphi(\varepsilon) \neq 0. \tag{74}$$

Alternatively, for some given $\alpha \geq 0$, τ can be expressed in terms of α as

$$\tau = g(\alpha) \triangleq \pi e\alpha^2 P^2(\mathbf{h}_\mathrm{B}^\mathrm{T}\mathbf{w}_\alpha)^2 + 3\pi e\sigma^2, \tag{75}$$

where $\mathbf{w}_\alpha$ is defined as

$$\mathbf{w}_\alpha \triangleq \operatorname*{argmax}_{\|\mathbf{w}\|_p \leq 1} \quad \mathbf{h}_\mathrm{B}^\mathrm{T}\mathbf{w} \tag{76a}$$

$$\text{s.t.} \quad |\mathbf{h}_\mathrm{E}^\mathrm{T}\mathbf{w}| \leq \alpha\mathbf{h}_\mathrm{B}^\mathrm{T}\mathbf{w}. \tag{76b}$$

Problem (76) is clearly equivalent to the perturbed problem in (66) when α and ε satisfy (74), or, equivalently, when α and τ satisfy (75). Thus, $\mathbf{h}_\mathrm{B}^\mathrm{T}\mathbf{w}_\alpha = \varphi(\varepsilon)$. Furthermore, we note from (76) that $\mathbf{h}_\mathrm{B}^\mathrm{T}\mathbf{w}_\alpha$ is nondecreasing with respect to α (increasing α relaxes the constraint in (76b)). Thus, $g(\alpha)$, as defined in (75), is a strictly increasing function of α. Substituting with $\tau = g(\alpha)$ back into (63) and changing the optimization variable into α, the problem in (63) can be written as

$$\operatorname*{maximize}_{\alpha} \ \frac{f(g(\alpha))}{g(\alpha)},$$

or, equivalently,

$$\operatorname*{maximize}_{\alpha} \ \frac{6P^2(\mathbf{h}_\mathrm{B}^\mathrm{T}\mathbf{w}_\alpha)^2 + 3\pi e\sigma^2}{\pi e\alpha^2 P^2(\mathbf{h}_\mathrm{B}^\mathrm{T}\mathbf{w}_\alpha)^2 + 3\pi e\sigma^2}, \tag{77}$$

where $\mathbf{w}_\alpha$ is as defined in (76). Since $f(\tau)/\tau$ is quasiconcave with respect to τ, and $\tau = g(\alpha)$ is strictly increasing with respect to α, we conclude that $f(g(\alpha))/g(\alpha)$ is quasiconcave with respect to α, and hence the problem in (77) is quasiconvex, i.e., quasiconcave maximization problem.

Finally, the search interval for optimal α can be lower-bounded by the smallest feasible α, given by

$$\alpha_{\min} = \min_{\mathbf{w},\alpha} \quad \alpha \tag{78a}$$

$$\text{s.t.} \quad \mathbf{h}_\mathrm{B}^\mathrm{T}\mathbf{w} = 1, \tag{78b}$$

$$|\mathbf{h}_\mathrm{E}^\mathrm{T}\mathbf{w}| \leq \alpha, \tag{78c}$$

and the upper bound $\alpha_{\max} = \sqrt{6/\pi e}$ is simply obtained by noting that $f(g(\alpha)) \geq g(\alpha)$, and thus $R_\mathrm{s} \geq 0$, only if $\alpha \leq \sqrt{6/\pi e}$, which completes the proof. ■

APPENDIX B
PROOF OF PROPOSITION 2

The proof is mostly along the same line as that in Appendix A. The max-min problem in (16) can be expressed as

$$\underset{\tau}{\text{maximize}} \ \frac{f(\tau)}{\tau}, \tag{79}$$

where $f(\tau)$ is defined as

$$f(\tau) \triangleq \max_{\|\mathbf{w}\|_p \le 1} \min_{\mathbf{h}_\mathrm{B} \in \mathcal{H}_\mathrm{B}} 6P^2(\mathbf{h}_\mathrm{B}^\mathrm{T}\mathbf{w})^2 + 3\pi e\sigma^2 \tag{80a}$$

$$\text{s.t.} \ |\mathbf{h}_\mathrm{E}^\mathrm{T}\mathbf{w}| \le \sqrt{\frac{\tau - 3\pi e\sigma^2}{\pi e P^2}} \quad \forall \mathbf{h}_\mathrm{E} \in \mathcal{H}_\mathrm{E}. \tag{80b}$$

Next, we define the perturbation function $\varphi(\varepsilon)$ as

$$\varphi(\varepsilon) \triangleq \max_{\|\mathbf{w}\|_p \le 1, t} \quad t \tag{81a}$$

$$\text{s.t.} \ \ |\mathbf{h}_\mathrm{B}^\mathrm{T}\mathbf{w}| \ge t \quad \forall \mathbf{h}_\mathrm{B} \in \mathcal{H}_\mathrm{B}, \tag{81b}$$

$$|\mathbf{h}_\mathrm{E}^\mathrm{T}\mathbf{w}| \le \varepsilon \quad \forall \mathbf{h}_\mathrm{E} \in \mathcal{H}_\mathrm{E}, \tag{81c}$$

where ε is defined as in (65). Note from (80) and (81) that $f(\tau) = 6P^2(\varphi(\varepsilon))^2 + 3\pi e\sigma^2$. Note also that, unlike (66), the perturbed problem in (81) is nonconvex because of the constraint in (81b). This nonconvexity can be eliminated by imposing the additional constraint

$$\mathbf{h}_\mathrm{B}^\mathrm{T}\mathbf{w} \ge 0 \quad \forall \mathbf{h}_\mathrm{B} \in \mathcal{H}_\mathrm{B}, \tag{82}$$

or, equivalently, replacing (81b) with

$$\mathbf{h}_\mathrm{B}^\mathrm{T}\mathbf{w} \ge t \quad \forall \mathbf{h}_\mathrm{B} \in \mathcal{H}_\mathrm{B}. \tag{83}$$

The additional constraint, however, may render the solution suboptimal. Let $\underline{\varphi}(\varepsilon)$ be defined as

$$\underline{\varphi}(\varepsilon) \triangleq \max_{\|\mathbf{w}\|_p \le 1, t} \quad t \tag{84a}$$

$$\text{s.t.} \ \ \mathbf{h}_\mathrm{B}^\mathrm{T}\mathbf{w} \ge t \quad \forall \mathbf{h}_\mathrm{B} \in \mathcal{H}_\mathrm{B}, \tag{84b}$$

$$|\mathbf{h}_\mathrm{E}^\mathrm{T}\mathbf{w}| \le \varepsilon \quad \forall \mathbf{h}_\mathrm{E} \in \mathcal{H}_\mathrm{E}. \tag{84c}$$

Then, $\underline{\varphi}(\varepsilon) \le \varphi(\varepsilon)$, i.e., a nonzero gap may exist between the two problems. In the sequel we show that this gap actually disappears with an additional technical assumption on $\mathcal{H}_\mathrm{B}$.

Lemma 1: If $\mathcal{H}_\mathrm{B}$ is convex, then $\underline{\varphi}(\varepsilon) = \varphi(\varepsilon)$, i.e., the problems in (81) and (84) are equivalent.

Proof: The proof is provided in Appendix C.

Following the same approach from Appendix A, it can be shown that $f(\tau) = 6P^2(\underline{\varphi}(\varepsilon))^2 + 3\pi e\sigma^2$ is concave with respect to τ, and thus $f(\tau)/\tau$ is quasiconcave. Next, we introduce the variable $\alpha \ge 0$ via the substitution

$$\tau = \pi e\alpha^2 P^2 t_\alpha^2 + 3\pi e\sigma^2, \tag{85}$$

where t_α is obtained from

$$(\mathbf{w}_\alpha, t_\alpha) = \underset{\|\mathbf{w}\|_p \le 1, t}{\text{argmax}} \quad t \tag{86a}$$

$$\text{s.t.} \ \ \mathbf{h}_\mathrm{B}^\mathrm{T}\mathbf{w} \ge t \quad \forall \mathbf{h}_\mathrm{B} \in \mathcal{H}_\mathrm{B}, \tag{86b}$$

$$|\mathbf{h}_\mathrm{E}^\mathrm{T}\mathbf{w}| \le \alpha t \quad \forall \mathbf{h}_\mathrm{E} \in \mathcal{H}_\mathrm{E}. \tag{86c}$$

Note from (84) and (86) that $t_\alpha = \underline{\varphi}(\varepsilon)$ whenever α and τ satisfy (85). Substituting (85) back into (79), the latter can be rewritten as

$$\underset{\alpha}{\text{maximize}} \ \frac{6P^2 t_\alpha^2 + 3\pi e\sigma^2}{\pi e\alpha^2 P^2 t_\alpha^2 + 3\pi e\sigma^2}. \tag{87}$$

Similar to (77) in Appendix A, we note from (85) and (86) that τ is strictly increasing with respect to α. Thus, the objective in (87) is quasiconcave with respect to α. Finally, $\alpha_{\min}$ can be obtained by modifying the problem in (78) to

$$\underset{\mathbf{w}, \alpha}{\text{minimize}} \ \ \alpha \tag{88a}$$

$$\text{s.t.} \ \ \mathbf{h}_\mathrm{B}^\mathrm{T}\mathbf{w} \ge 1 \quad \forall \mathbf{h}_\mathrm{B} \in \mathcal{H}_\mathrm{B}, \tag{88b}$$

$$|\mathbf{h}_\mathrm{E}^\mathrm{T}\mathbf{w}| \le \alpha \quad \forall \mathbf{h}_\mathrm{E} \in \mathcal{H}_\mathrm{E}, \tag{88c}$$

which completes the proof. ■

APPENDIX C
PROOF OF LEMMA 1

Let the pair $(\mathbf{w}^*, t^*)$ be an optimal solution of the nonconvex perturbed problem in (81), where $t^* = \varphi(\varepsilon)$. If $\mathcal{H}_\mathrm{B}$ is convex, then the linear function $f_{\mathbf{w}^*}(\mathbf{h}_\mathrm{B}) \triangleq \mathbf{h}_\mathrm{B}^\mathrm{T}\mathbf{w}^*$ maps $\mathcal{H}_\mathrm{B}$ into an interval with three possible outcomes:

1) If $\mathbf{h}_\mathrm{B}^\mathrm{T}\mathbf{w}^* \ge 0$ for all $\mathbf{h}_\mathrm{B} \in \mathcal{H}_\mathrm{B}$, then $t^* \ge 0$.
2) If $\mathbf{h}_\mathrm{B}^\mathrm{T}\mathbf{w}^* \le 0$ for all $\mathbf{h}_\mathrm{B} \in \mathcal{H}_\mathrm{B}$, then $t^* \ge 0$. This also implies that $-\mathbf{h}_\mathrm{B}^\mathrm{T}\mathbf{w}^* \ge 0$ for all $\mathbf{h}_\mathrm{B} \in \mathcal{H}_\mathrm{B}$. Note that if $(\mathbf{w}^*, t^*)$ is a solution to (81), then $(-\mathbf{w}^*, t^*)$ is also a solution.
3) If there exist $\mathbf{h}_1, \mathbf{h}_2 \in \mathcal{H}_\mathrm{B}$ such that $\mathbf{h}_1^\mathrm{T}\mathbf{w}^* > 0 > \mathbf{h}_2^\mathrm{T}\mathbf{w}^*$, then $t^* = 0$.

From the above cases, we see that $\mathbf{h}_\mathrm{B}^\mathrm{T}\mathbf{w}^* \ge 0$, or $\mathbf{h}_\mathrm{B}^\mathrm{T}\mathbf{w}^* \le 0$, for all $\mathbf{h}_\mathrm{B} \in \mathcal{H}_\mathrm{B}$, is a necessary condition to obtain nonzero t^*. Thus, we lose nothing by imposing the constraint in (82), provided that $\mathcal{H}_\mathrm{B}$ is a convex set. ■

APPENDIX D
COMPONENTS OF $\mathbf{h_0}$ AND $\mathbf{J_0}$ FROM (28)

From (26), for $i = 1, \ldots, N$, $c_i \ne 0$, we have

$$\frac{1}{c_i} h_i(\boldsymbol{\delta}) = \frac{(d_z - \delta_z)^m (\mathbf{d}_i - \boldsymbol{\delta})^\mathrm{T}\mathbf{u}}{\|\mathbf{d}_i - \boldsymbol{\delta}\|_2^{m+3}}, \tag{89a}$$

$$\frac{1}{c_i}\frac{\partial h_i(\boldsymbol{\delta})}{\partial \delta_x} = \frac{-(d_z - \delta_z)^m \mathbf{e}_1^\mathrm{T}\mathbf{u}}{\|\mathbf{d}_i - \boldsymbol{\delta}\|_2^{m+3}} + \frac{(m+3)(d_{x,i} - \delta_x)(d_z - \delta_z)^m (\mathbf{d}_i - \boldsymbol{\delta})^\mathrm{T}\mathbf{u}}{\|\mathbf{d}_i - \boldsymbol{\delta}\|_2^{m+5}}, \tag{89b}$$

$$\frac{1}{c_i}\frac{\partial h_i(\boldsymbol{\delta})}{\partial \delta_y} = \frac{-(d_z - \delta_z)^m \mathbf{e}_2^\mathrm{T}\mathbf{u}}{\|\mathbf{d}_i - \boldsymbol{\delta}\|_2^{m+3}} + \frac{(m+3)(d_{y,i} - \delta_y)(d_z - \delta_z)^m (\mathbf{d}_i - \boldsymbol{\delta})^\mathrm{T}\mathbf{u}}{\|\mathbf{d}_i - \boldsymbol{\delta}\|_2^{m+5}}, \tag{89c}$$

$$\frac{1}{c_i}\frac{\partial h_i(\boldsymbol{\delta})}{\partial \delta_z} = \frac{-m(d_z - \delta_z)^{m-1}(\mathbf{d}_i - \boldsymbol{\delta})^\mathrm{T}\mathbf{u} - (d_z - \delta_z)^m \mathbf{e}_3^\mathrm{T}\mathbf{u}}{\|\mathbf{d}_i - \boldsymbol{\delta}\|_2^{m+3}} + \frac{(m+3)(d_z - \delta_z)^{m+1}(\mathbf{d}_i - \boldsymbol{\delta})^\mathrm{T}\mathbf{u}}{\|\mathbf{d}_i - \boldsymbol{\delta}\|_2^{m+5}}, \tag{89d}$$

where $\mathbf{e}_j, j = 1, 2, 3$, is the jth column of $\mathbf{I}_3$. Substituting with $\boldsymbol{\delta} = \mathbf{0}$ back into (89), we obtain

$$h_i(\mathbf{0}) = c_i \frac{d_z^m \mathbf{d}_i^{\mathrm{T}} \mathbf{u}}{\|\mathbf{d}_i\|_2^{m+3}}, \tag{90a}$$

$$\frac{\partial h_i(\mathbf{0})}{\partial \delta_x} = c_i \left(\frac{-d_z^m \mathbf{e}_1^{\mathrm{T}}}{\|\mathbf{d}_i\|_2^{m+3}} + \frac{(m+3) d_{x,i} d_z^m \mathbf{d}_i^{\mathrm{T}}}{\|\mathbf{d}_i\|_2^{m+5}} \right) \mathbf{u}, \tag{90b}$$

$$\frac{\partial h_i(\mathbf{0})}{\partial \delta_y} = c_i \left(\frac{-d_z^m \mathbf{e}_2^{\mathrm{T}}}{\|\mathbf{d}_i\|_2^{m+3}} + \frac{(m+3) d_{y,i} d_z^m \mathbf{d}_i^{\mathrm{T}}}{\|\mathbf{d}_i\|_2^{m+5}} \right) \mathbf{u}, \tag{90c}$$

$$\frac{\partial h_i(\mathbf{0})}{\partial \delta_z} = c_i \left(\frac{-m d_z^{m-1} \mathbf{d}_i^{\mathrm{T}} - d_z^m \mathbf{e}_3^{\mathrm{T}}}{\|\mathbf{d}_i\|_2^{m+3}} + \frac{(m+3) d_z^{m+1} \mathbf{d}_i^{\mathrm{T}}}{\|\mathbf{d}_i\|_2^{m+5}} \right) \mathbf{u}. \tag{90d}$$

REFERENCES

[1] A. D. Wyner, "The wire-tap channel," *Bell System Technical Journal*, vol. 54, pp. 1355–1387, 1975.

[2] Y. Liang, H. V. Poor, and S. Shamai (Shitz), *Information Theoretic Security*, ser. Foundations and Trends® in Communications and Information Theory. Now Publishers, 2008, vol. 5, no. 4-5.

[3] M. Bloch and J. Barros, *Physical-Layer Security: From Information Theory to Security Engineering*. Cambridge University Press, 2011.

[4] A. Mukherjee, S. Fakoorian, J. Huang, and A. Swindlehurst, "Principles of physical layer security in multiuser wireless networks: A survey," *IEEE Commun. Surveys Tuts.*, vol. 16, no. 3, pp. 1550–1573, 3rd Quart. 2014.

[5] A. Mukherjee, "Physical-layer security in the internet of things: Sensing and communication confidentiality under resource constraints," *Proceedings of the IEEE*, vol. 103, no. 10, pp. 1747–1761, Oct. 2015.

[6] T. Komine and M. Nakagawa, "Fundamental analysis for visible-light communication system using LED lights," *IEEE Transactions on Consumer Electronics*, vol. 50, no. 1, pp. 100–107, 2004.

[7] A. Mostafa and L. Lampe, "Physical-layer security for MISO visible light communication channels," *IEEE Journal on Selected Areas in Communications*, vol. 33, no. 9, pp. 1806–1818, Sept. 2015.

[8] Z. Li, W. Trappe, and R. Yates, "Secret communication via multi-antenna transmission," in *41st Annual Conference on Information Sciences and Systems*, March 2007, pp. 905–910.

[9] S. Shafiee and S. Ulukus, "Achievable rates in Gaussian MISO channels with secrecy constraints," in *IEEE International Symposium on Information Theory*, June 2007, pp. 2466–2470.

[10] A. Khisti and G. W. Wornell, "Secure transmission with multiple antennas I: The MISOME wiretap channel," *IEEE Trans. Inf. Theory*, vol. 56, no. 7, pp. 3088–3104, 2010.

[11] F. Oggier and B. Hassibi, "The secrecy capacity of the MIMO wiretap channel," *IEEE Trans. Inf. Theory*, vol. 57, no. 8, pp. 4961–4972, Aug. 2011.

[12] L. Zhang, Y. C. Liang, Y. Pei, and R. Zhang, "Robust beamforming design: From cognitive radio MISO channels to secrecy MISO channels," in *IEEE Global Telecommunications Conference*, Nov 2009, pp. 1–5.

[13] W. Shi and J. Ritcey, "Robust beamforming for MISO wiretap channel by optimizing the worst-case secrecy capacity," in *Forty Fourth Asilomar Conference on Signals, Systems and Computers*, Nov 2010, pp. 300–304.

[14] Q. Li and W. K. Ma, "Optimal and robust transmit designs for MISO channel secrecy by semidefinite programming," *IEEE Trans. Signal Process.*, vol. 59, no. 8, pp. 3799–3812, Aug. 2011.

[15] J. Huang and A. Swindlehurst, "Robust secure transmission in MISO channels based on worst-case optimization," *IEEE Trans. Signal Process.*, vol. 60, no. 4, pp. 1696–1707, April 2012.

[16] K. Cumanan, Z. Ding, B. Sharif, G. Y. Tian, and K. K. Leung, "Secrecy rate optimizations for a MIMO secrecy channel with a multiple-antenna eavesdropper," *IEEE Trans. Veh. Technol.*, vol. 63, no. 4, pp. 1678–1690, May 2014.

[17] Z. Chu et al., "Secrecy rate optimizations for a MIMO secrecy channel with a cooperative jammer," *IEEE Trans. Veh. Technol.*, vol. 64, no. 5, pp. 1833–1847, May 2015.

[18] N. Jindal, "MIMO broadcast channels with finite-rate feedback," *IEEE Trans. Inf. Theory*, vol. 52, no. 11, pp. 5045–5060, Nov. 2006.

[19] H. Elgala, R. Mesleh, and H. Haas, "Predistortion in optical wireless transmission using OFDM," in *Ninth International Conference on Hybrid Intelligent Systems*, vol. 2, Aug 2009, pp. 184–189.

[20] J. Grubor, S. Randel, K. D. Langer, and J. W. Walewski, "Broadband information broadcasting using LED-based interior lighting," *Journal of Lightwave Technology*, vol. 26, no. 24, pp. 3883–3892, Dec 2008.

[21] J. Kahn and J. Barry, "Wireless infrared communications," *Proceedings of the IEEE*, vol. 85, no. 2, pp. 265–298, Feb. 1997.

[22] O. Ozel, E. Ekrem, and S. Ulukus, "Gaussian wiretap channel with amplitude and variance constraints," *IEEE Trans. Inf. Theory*, vol. 61, no. 10, pp. 5553–5563, Oct. 2015.

[23] A. Ben-Tal and A. Nemirovski, "Robust convex optimization," *Mathematics of Operations Research*, vol. 23, no. 4, pp. 769–805, Nov. 1998.

[24] S. Boyd and L. Vandenberghe, *Convex Optimization*. Cambridge University Press, 2009.

[25] A. Ben-Tal and A. Nemirovski, "Robust solutions to uncertain linear programs," *Operations Research Letters*, vol. 25, pp. 1–13, 1999.

[26] ——, "Robust optimization – methodology and applications," *Math. Program., Ser. B 92:*, pp. 453–480, 2002.

[27] M. Grant and S. Boyd, "CVX: Matlab software for disciplined convex programming, version 2.1," http://cvxr.com/cvx, Mar. 2014.

[28] J. Gondzio, "Interior point methods 25 years later," *European Journal of Operational Research*, vol. 218, no. 3, pp. 587–601, 2012.

[29] M. ApS, *The MOSEK optimization toolbox for MATLAB manual. Version 7.1 (Revision 28).*, 2015. [Online]. Available: http://docs.mosek.com/7.1/toolbox/index.html

[30] R. Lenk and C. Lenk, *Practical Lighting Design With LEDs*. Wiley, 2011.

[31] L. Zeng et al., "High data rate multiple input multiple output (MIMO) optical wireless communications using white LED lighting," *IEEE JSAC*, vol. 27, no. 9, pp. 1654–1662, 2009.

[32] F. J. López-Hernández et al., "Ray-tracing algorithms for fast calculation of the channel impulse response on diffuse IR wireless indoor channels," *Opt. Eng.*, vol. 30, no. 10, pp. 2775–2780, Oct. 2000.

[33] J. V. Tiel, *Convex Analysis: An Introductory Text*. John Wiley & Sons, 1984.

[34] R. T. Rockafellar, *Convex Analysis*. Princeton University Press, 1970.

Ayman Mostafa (S'08) received the B.Sc. degree (with honours) in electrical engineering from Alexandria University, Egypt, in 2006, and the M.A.Sc. degree in electrical engineering from McMaster University, Hamilton, ON, Canada, in 2012. He is currently working towards the Ph.D. degree in electrical engineering at The University of British Columbia, Vancouver, BC, Canada. His current research interests are in the areas of physical-layer security, robust optimization, and optical wireless communications.

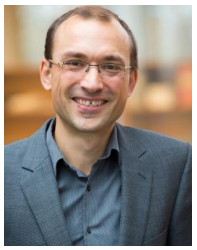

Lutz Lampe (M'02, SM'08) received the Dipl.-Ing. and Dr.-Ing. degrees in electrical engineering from the University of Erlangen, Germany, in 1998 and 2002, respectively. Since 2003, he has been with the Department of Electrical and Computer Engineering, The University of British Columbia, Vancouver, BC, Canada, where he is a Full Professor. His research interests are broadly in theory and application of wireless, power line, optical wireless and optical fibre communications. Dr. Lampe was the General (Co-)Chair for 2005 International Conference on Power Line Communications and Its Applications (ISPLC), 2009 IEEE International Conference on Ultra-Wideband (ICUWB) and 2013 IEEE International Conference on Smart Grid Communications (SmartGridComm). He is currently an Associate Editor of the IEEE WIRELESS COMMUNICATIONS LETTERS and the IEEE COMMUNICATIONS SURVEYS AND TUTORIALS and has served as an Associate Editor and a Guest Editor of several IEEE transactions and journals. He was a (co-)recipient of a number of best paper awards, including awards at the 2006 IEEE ICUWB, the 2010 IEEE International Communications Conference (ICC), and the 2011 IEEE ISPLC. He is co-editor of the book Power Line Communications: Principles, Standards and Applications from Multimedia to Smart Grid, published by John Wiley & Sons in its 2nd edition in 2016.